Study of the effect of mitochondrial deficiency on the neuronal morphology of the nematode *Caenorhabditis elegans*

Dissertation

zur

Erlangung des Doktorgrades (Dr. rer. nat.)

der

Mathematisch-Naturwissenschaftlichen Fakultät

der

Rheinischen Friedrich-Wilhelms-Universität Bonn

vorgelegt von

Anna Gioran

aus Athen

Bonn, Dezember 2014

Angefertigt mit Genehmigung der Mathematisch-Naturwissenschaftlichen Fakultät der
Rheinischen Friedrich-Wilhelms-Universität Bonn

1. Gutachter: Prof. Dr. Pierluigi Nicotera

2. Gutachter: Prof. Dr. Michael Hoch

Tag der Promotion: 21.04.2015

Erscheinungsjahr: 2015

To my parents,

Ioakeim & Ainta

Table of Contents

1. Summary

Neurons are highly polarized cells that constantly undergo remodeling of their branches during and after their development. This energy demanding process depends on energy provision from mitochondria via the oxidative phosphorylation (OXPHOS). Although the molecular mechanisms connecting the two are important for understanding pathologies linked to defective neuronal branching due to mitochondrial deficiency, they still remain elusive. In this study, we approached this problem by using as a model a highly branched sensory neuron in *Caenorhabditis elegans* which demonstrates altered branching pattern in conditions of mitochondrial deficiency. In particular, we show that animals carrying mutations in genes encoding mitochondrial complex I subunits have more dendrites on their sensory neurons compared to wild type animals. The increased outgrowth is not a cell type-specific phenomenon since other types of sensory neurons demonstrate ectopic structures due to complex I deficiency, as well. Importantly, the increased branching is not a result of oxidative stress, but it is regulated by a distinct signaling cascade. Specifically, activation of AMP-activated protein kinase AMPK due to mitochondrial deficiency is one of the regulatory events and we show that its downstream target phosphoinositide 3-kinase PI3K participates in the same pathway. Finally, we demonstrated that the increased neuronal arborizations displayed by OXPHOS mutants are independent of their longevity. Overall, our findings reveal a signaling pathway which regulates tightly dendritic branching in conditions of mitochondrial deficiency and contribute to the understanding of more complicated phenomena occurring in relevant neurodegenerative diseases.

2. Introduction

2.1 Neuronal morphology and neurodegeneration

Ever since Santiago Ramón y Cajal, the founder of neuroscience, described the organization of the neurons and the vertebrate nervous system in the late 1800s, the scientific community is aware of the complicated shape of these cells and their intense polarization [1]. Indeed the neurons display a high degree of morphological and functional polarization. Neurons are characterized by the presence of neuronal projections or neurites which mostly include a long thin axon and shorter dendrites. Additionally, dendrites carry spines on their surface which are small outgrowths and receive synaptic input. This high polarization is essential for the determination of the direction of the signal flow in neurons [2]. Therefore, the formation and maintenance of a neuron's projections are directly linked to its functionality.

The process of forming and maintaining neuronal projections is firmly orchestrated and it requires a big variety of branching determinants and accompanying proteins as well as a significant amount of energy [3, 4]. In addition, neurons undergo morphological changes due to stimuli from their environment which includes other neurons [3, 4]. This leads to neuronal circuit formation and their maintenance as well as their plasticity are of pivotal importance for the proper function of the brain [5]. Taking the above under consideration, it is expected that compromised structural integrity of the neurons can lead to defective communication between the neurons of a circuit which can eventually affect the function of the entire brain and result into cognitive impairment.

Alterations in neuronal morphology are associated with neurodegenerative diseases that can lead to cognitive impairment. Despite the fact that neurodegenerative diseases alter neurite and spine morphology, the mechanisms connecting neurodegenerative diseases and alterations in neuronal morphology as well as the causative relation between them are not well understood. Several neurodegenerative diseases like Alzheimer's and Parkinson's have been shown to implicate reorganization of dendritic structures. Briefly, Alzheimer's disease is the most common form of dementia [6] and it is histologically characterized by the formation of amyloid plaques and neurofibrillary tangles. The main component of the plaques is the Aβ amyloid which is formed by small peptides of 40-42 amino acids called Aβ42 [7]. The neurofibrillary tangles consist of tau protein which aggregates into insoluble fibrillar deposits when it is hyperphoshorylated [8]. On the other hand, Parkinson's disease causes loss of dopaminergic neurons in a specific brain area, namely the substantia nigra, and leads to diminishing of the control over voluntary movement [9]. Histologically, this disease is

characterized by neuronal inclusions, the Lewy bodies and the Lewy neurites [10]. Both types of inclusions contain a pre-synaptic protein, α-synuclein, in an aggregated, oligomeric or fibrillar form [11]. Both Alzheimer's and Parkinson's diseases result into reorganization of dendritic branching in basal forebrain neurons of patients [12]. Additionally, it has been also proposed that degenerating neurites represent a cause rather than a consequence of Aβ accumulation in late-onset Alzheimer's [13].

Another example of a neurodegenerative disease that leads to neuronal loss and remodeling is Huntington's disease. Huntington's disease is inherited in an autosomal dominant manner and it occurs due to expansion of a CAG trinucleotide repeat in the huntingtin (HTT) gene which results into an expanded polyglutamine stretch in the HTT protein. The disease is histologically characterized by loss of specific neuronal subpopulations in the cortex and striatum [14] and clinically by chorea, cognitive impairment and psychiatric disorders [15]. Regarding the neurite remodeling associated with Huntington's disease, striatal neurons from patients were found to have both degenerative and proliferative changes such as increased numbers and size of dendritic spines, short-segment branching along dendrites and truncated dendritic arborizations [16, 17].

Although the neurodegenerative diseases discussed above as well as others occur with high frequencies [18], the mechanisms underlying the involved neurite degeneration remain obscure. Therefore, there is an urgent need for understanding these mechanisms.

2.2 Role of mitochondria in neurodegeneration

Neurons need to form and maintain a specific shape in order to be functional and able to communicate with the neurons of the circuits they belong to. A great variety of factors is responsible for the shaping of the neurons. In many different ways, mitochondria have also been implicated in this process and as consequence, in neurodegeneration [19].

Mitochondria produce energy through the oxidative phosphorylation. The oxidative phosphorylation is the metabolic pathway whose end product is ATP, the molecule that funnels energy into metabolism. Five main protein complexes (Complexes I-V) are involved in the energy production and they comprise an electron transport chain system. These complexes are embedded in the inner mitochondrial membrane and the electron transport generates a proton gradient which is exploited by ATP synthase (Complex V) that forms ATP

from ADP and inorganic phosphate in a phosphorylation reaction [20]. Among other cellular processes, neurons require energy to form and maintain their projections. Indeed, ATP level reduction has been shown to result in defective dendrite morphogenesis. For example, downregulation of the Cytoplasmic Polyadenylation Element Binding protein 1 (CPEB1) which is responsible for the transcription of an mRNA encoding one of the subunits of Complex I, causes reduction of the ATP production. This reduction led to reduced neurite formation of primary neurons from CPEB1 knockout mice compared to wild type animals [21].

Secondly, mitochondria are dynamic organelles undergoing circles of fusion and fission. Overall mitochondria form mostly tubular networks inside the cells and these networks can shift their shape in response to certain stimuli [22]. Fusion and fission are the two processes that sculpt the mitochondrial network and their physiological role has been linked to mitochondrial integrity maintenance, proliferation, as well as content exchange such as mitochondrial DNA [23]. It has been demonstrated that fusion and fission occurs in neurons as a means of distribution of mitochondria in neurites. This distribution occurs in response to neuronal activity and it is correlated with synaptogenesis, neurite and spine formation. Indeed, neurons that have defective fission mechanisms do not form small mitochondrial fragments that can be transferred to the thin neuronal projections and assist with the local needs of the projection. Mitochondria depleted projections have fewer spines and synapses and these neurons form fewer neurites as shown by studies on hippocampal [24], cultured forebrain neurons [25] and Purkinje cells [26].

Apart from fusion and fission, mitochondria are distributed inside the cell via active transportation, (mitochondrial trafficking). Adaptor proteins and kinesins form complexes in order to achieve mitochondrial transportation via the microtubules to the loci where the energy demands require the presence of mitochondria [22, 27]. It has been demonstrated that immobilization of mitochondria can have an impact on neurite formation and specifically axon branching. In particular, it was shown both *in vivo* and *in vitro* that two kinases, LKB1 and NUAK1 are necessary and sufficient to immobilize mitochondria at nascent presynaptic sites. This immobilization is of vital importance for the branching stimulation since mobile mitochondria are not able to induce branching [28].

Considering the effect the disruptions of the mitochondrial function can have on the morphology of neurons, it is only logical to hypothesize that mitochondrial deficiencies might be involved in neurodegenerative diseases. Indeed, mutations in mitochondrial DNA and

oxidative stress contribute to ageing which is the greatest risk factor for the onset of neurodegeneration and evidence suggests that mitochondrial dysfunction may occur early and act causally in neurodegenerative diseases [29]. Moreover, patients having mitochondrial deficiencies manifest a variety of symptoms most of which are of neurological nature [30], a fact which highlights even more the importance of intact mitochondria for proper neuronal function.

Several studies have found that mitochondrial dysfunction and oxidative damage can contribute to the pathogenesis of Alzheimer's disease [31, 32]. In addition, defective trafficking of organelles, including mitochondria was found in autoptic patients with sporadic Alzheimer's [33]. Abnormal mitochondrial dynamics are present in Alzheimer's disease models and are thought to contribute to the pathology [34]. Finally, evidence from a mouse model of Alzheimer's disease confirmed the implication of decreased anterograde mitochondrial movement, increased mitochondrial fission and decreased fusion, defective mitochondrial function as well as impaired mitochondrial biogenesis in primary neurons of these mice [35].

Inhibition of the mitochondrial complex I has been found to be relevant in naturally occurring Parkinson's disease since complex I deficiency was found in the substantia nigra of patients with either idiopathic or pre-symptomatic Parkinson's disease [36]. Moreover, although there are some discrepancies in the reported phenotypes, mitochondrial dynamics seem to be affected in different models of Parkinson's disease or in tissues from patients [37].

Disturbance of almost all of the mitochondrial functions has been involved in the pathophysiology of Huntington's disease [38, 39]. Specifically, it is thought that the mutant huntingtin directly associates with mitochondria since it has been found that it can bind on the outer mitochondrial membrane [40] and interferes with certain mitochondrial functions such as protein import [41]. Examination of postmortem brain samples from Huntington's patients revealed decreased activity of complexes II and III [42]. Moreover, as recently demonstrated, the mutant huntingtin interacts with a mediator of mitochondrial fission (Dynamin-related protein-Drp1) leading to excessive fragmentation of mitochondria and thus to neuronal damage [43].

Although there is accumulating evidence regarding the correlation of mitochondrial dysfunction and neurodegenerative diseases, it is not yet clear in most of the cases if mitochondrial dysfunction is a causal or a consequential effect for each neurodegenerative

disease. In addition, little is known about the signaling pathways that mediate the neurodegeneration due to mitochondrial deficiencies.

2.3 *Caenorhabditis elegans* as a model organism

Caenorhabditis elegans is a free living (non-parasitic) nematode. The species belongs to the Phylum Nematoda, Class Chromadorea, Order Rhabditida, Family Rhabditidae and Genus Caenorhabditis (Maupas, É. "Modes et forms de reproduction des nématodes", 1900).

C. elegans was firstly introduced as a model organism in 1974 by Sydney Brenner. His work focused mostly on establishing the basic genetic features of the organism as well as on the development of methods for determining the structure of its nervous system [44]. Ever since, *C. elegans* has been extensively used as a model organism in the fields of ageing [45, 46], neurobiology [47, 48], developmental biology [49], immunology [50, 51], biomedicine [52, 53] and others. The level of its characterization as a model is highlighted by the number of existing databases and tools that are available online. Some examples are the Wormatlas (http://www.wormatlas.org/) which is a database of behavioral and structural anatomy of *C. elegans*, the Wormbase (http://www.wormbase.org) which contains *C. elegans* gene information with links to all available data for the respective genes, available mutant strains etc and the Wormweb (http://wormweb.org/neuralnet) which provides all the information about the mapping of the nervous system of the organism.

The extensive use of this simple model stems from the fact that it gathers a series of features and advantages that makes it particular. First of all, *C. elegans* homologues have been identified for ~80% of human genes [54] a fact that makes it a model relevant for investigations on human pathophysiology [55]. Regarding its maintenance in the laboratory, *C. elegans* is inexpensive and easy to handle. Its small size (~1 mm) and inexpensive maintenance materials along with its self-fertilizing reproduction mode allow culturing of large numbers of nematodes and of several strains simultaneously. Additionally, its short life cycle (4 days at 20ºC for wild type animals- Image 1) and short life span (approximately 30 days at 20ºC for wild type animals) make it ideal for ageing studies. Moreover, the availability of mutant strains and RNAi constructs make *C. elegans* attractive for epistasis analyses and studies that require genetic approaches. In addition, the two strategies widely used for transgenesis in *C. elegans* are efficient and fast and both deliver exogenous DNA in

the worm's germline. This is done either by microinjecting DNA directly in the germline which leads to the generation of extrachromosomal arrays consisting of several copies of the transgene, or by conducting biolistic transformation (bombardment) which results into integration of the transgene in the genome in low copy numbers [56]. Last but not least, all the mutant or transgenic strains can be maintained for several years since young larvae can survive freezing and thawing.

2.4 The nervous system of *C. elegans*

The *C. elegans* nervous system, which will be the focusing point of this study, has been extensively studied ever since the introduction of the model. In his first studies Sydney Brenner reported numerous observations on the neuronal mapping and nervous system organization of the roundworm [44]. The most complex tissue of *C. elegans* is its nervous system, and in fact, it comprises about one third of the total somatic cells of the adult worm (302 out of 959 in the hermaphrodite and 381 out of 1031 in the male). Reconstructions of electron micrographs have provided a full structure and connectivity map; 20 neurons are located in the pharynx and the rest in various ganglia in the head, tail and along the ventral cord (Image 2). Almost all of the neurons are morphologically simple with few or no branches [57]. *C. elegans* has sensory, motor and interneurons [57] as well as some glial cells [58] that participate in the organization of the nervous system.

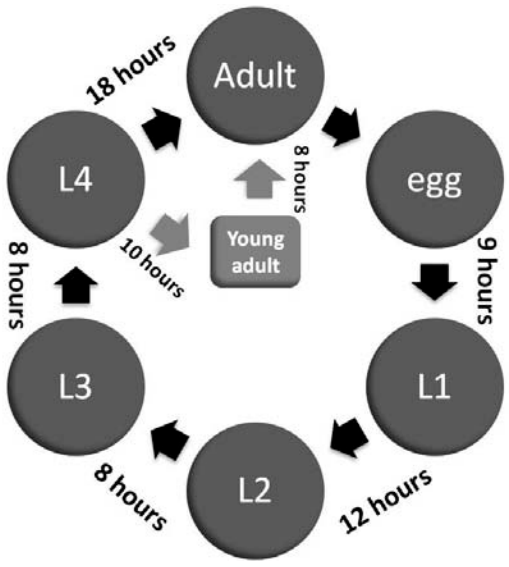

Image 1: Schematic showing the life cycle of wild type *C. elegans* at 22ºC. The adult animal is capable of laying ~300 eggs which hatch and give stage 1 larvae (L1). After 4 molting steps and about 3 days, the L1s reach the adulthood, thus completing the life cycle of this nematode.

What makes the study of the worm nervous system so attractive is firstly the transparency of its body which allows imaging of the neurons and secondly, the display of certain behavioral modalities which can be monitored to assess neuronal functionality. In addition, the introduction of the concept of expressing under tissue- or cell-specific promoters LacZ initially and the green fluorescent protein (GFP) later, enabled the tagging of single or groups of neurons, thus providing more information regarding details of their structure and development [59, 60]. Moreover, many characteristics present in the roundworm nervous system are found in mammalian neurons as well.

For example, the *C. elegans* nervous system displays morphological alterations due to ageing [61-63], it possesses mechanisms of neuronal regeneration [64] and mechanisms of neuronal pruning [65], processes which occur in mammalian neurons as well and are relevant for pathological conditions of the nervous system. Lastly, neurotransmitter receptors, neurotransmitter synthesis and release pathways are highly conserved between *C. elegans* and mammals [66]. These similarities make *C. elegans* a model organism attractive for neurobiology studies relevant to human neuropathology.

As mentioned earlier, *C. elegans* also exerts certain behavioral patterns which can be utilized to assess neuronal functionality and reveal the neurons that participate in certain circuits. One noteworthy example is the "basal slow response" which describes the slow-down of locomotion that well fed animals display when they encounter a bacterial lawn. This behavior is mediated by dopaminergic neurons, thus failure to exert this specific behavior can be linked to defective function of these neurons [67]. Moreover, several other behavioral paradigms in *C. elegans* such as odortaxis, thermotaxis and male mating have enabled us to identify genes that alter them as well as the neural circuits underlying each behavior [68].

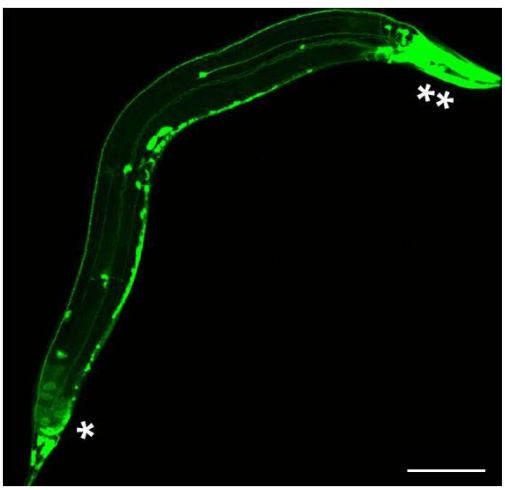

Image 2: Image of a live worm expressing GFP under a pan-neuronal promoter. The single asterisk indicates the tail and the double asterisk the head. The cephalic (or head) ganglia as well as several neurons in the rest of body are clearly shown in the image. The strain is the OH441: *otIs45* [*unc-119*::*gfp*]. The scale bar represents 25 μm.

In this study we focused mainly on the PVD neurons. The PVD neurons (PVDL and PVDR) are mechanosensory - nociception neurons [57, 69]. They are born post-embryonically and they mediate an avoidance response to harsh touch [59]. It has been shown that these neurons can have a proprioception function as well, since their ablation can affect the posture of the animal [70]. In the adult animal the PVDs are fully developed and they envelop almost the entire body of the nematode.

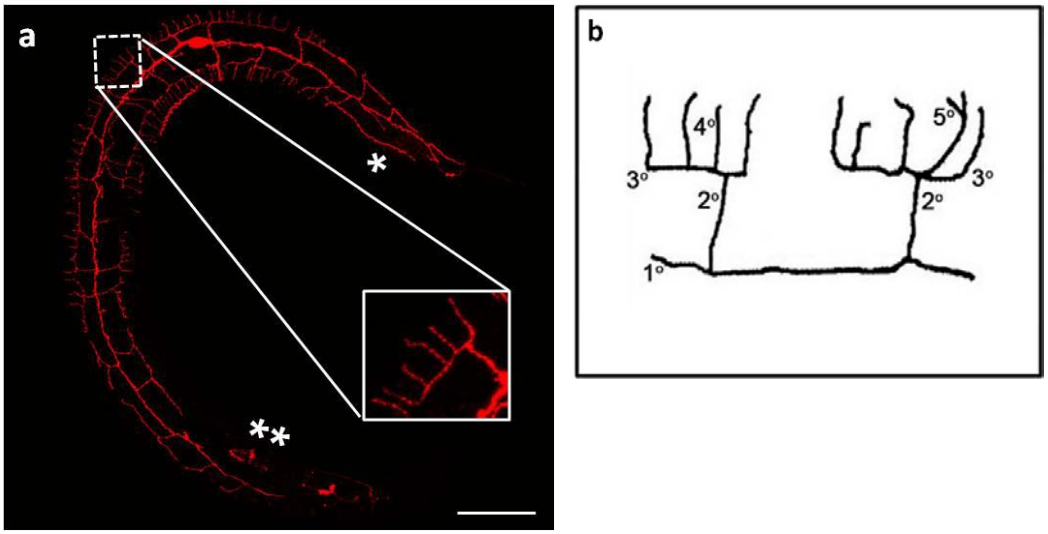

Image 3: The PVD neurons display an elaborate dendritic branching pattern. **a)** The PVD neuron of a late L4 animal. The development of the neurons is already complete and apart from the very posterior area the entire body in enveloped by both PVD neurons. The insert shows a "menorah" which is the repetitive structural unit of the neuron. The scale bar represents 25 μm. **b)** Schematic of the structure of two neighboring menorahs where the degrees of the branches are indicated.

They demonstrate an elaborate branching pattern that consists of a certain number (~40 per animal) of non-overlapping repetitive structures (Image 3a). These repetitive structures are called "menorahs" because of their resemblance with candelabra and they follow a specific pattern during their development. The stem of each menorah (2º branch) grows on a primary branch (1º branch) which stems directly from the cell body and runs throughout almost the entire body of the nematode. When the 2º branches reach a certain size, they turn 90º and continue to grow thus forming the 3º branches. Finally, on the 3º branch 4º processes grow

(Image 3b). Most of the menorahs stop their development at this point although occasionally 5º or 6º branches may appear.

The structural complexity of this neuron has been proved to be a valuable tool for assessing roles of variable proteins in dendritic branch formation. For example, study of its tiling properties has revealed that netrin (UNC-6) regulates this process and prevents the overlapping of neighboring (or sister) dendrites [71]. Furthermore, novel complexes of membrane adhesion molecules have been revealed through the study of the PVD neuron. Reportedly, DMA-1, a transmembrane protein, is expressed on the PVD neuron and by binding to a ligand complex (SAX-7/L1CAM), which is expressed in the surrounding hypodermal tissue, it mediates branching of the neuron [72, 73]. Finally, cell-specific expression profiling of the PVD has uncovered a big portion of molecules that mediate its branching [69]. Although a deeper investigation is required on the data of this profiling, the information collected to this point as well as the PVD neuron itself, provide a promising model for identification of evolutionarily conserved branching determinants.

2.5 *C. elegans* as a model to study neurodegeneration

As previously discussed, *C. elegans* has a very well-defined nervous system and along with its utilization as a genetic model, it offers an effective platform to elucidate basic mechanistic pathways that underlie complex human neurodegenerative diseases. In fact, *C. elegans* has been extensively used to model and study neurodegeneration [74-76].

Alzheimer's disease has been modeled and studied in *C. elegans*. Although *C. elegans* does not have tau and it does not generate Aβ peptides, heterologous expression of the human proteins is possible. Indeed, transgenic worms that express Aβ42 in pan-neuronal manner human have defective odorant preferences, associative learning behavior, experience-dependent learning as well as egg laying [77]. Apart from heterologous expression systems, *C. elegans* can facilitate studying of Alzheimer's in a homologous manner since it carries the *apl-1* gene which encodes for the APL-1 (amyloid precursor-like protein) and it is the homolog of the APP human protein. In pathological conditions APP is cleaved by certain proteases and Aβ is produced which forms the plaques and leads to the disease onset. The *C. elegans* APL-1 lacks the protease cleaving site therefore Aβ cannot be produced [78].

Nevertheless, a role for APL-1 in the nervous system of *C. elegans* has been found, specifically in regulating transmission at the body wall neuromuscular junction [79].

Similarly to Alzheimer's disease, *C. elegans* lacks the orthologues of genes related to Parkinson's disease such as α-synuclein. Nevertheless, some work has been done to model and study Parkinson's in the worm through transgenic expression of human genes. Indeed, animals overexpressing human α-synuclein in dopaminergic neurons display loss of these neurons and defects the "basal slowing response" (see above) [80]. Alpha-synuclein is not the only culprit in Parkinson's disease. Another gene commonly found to be mutated in familial Parkinson's disease is the one encoding for the leucine-rich repeat kinase 2 (LRRK2) [81]. Overexpression of the human LRRK2 in selective neurons of *C. elegans* leads to degeneration of dopaminergic neurons [82].

Finally, Huntington's disease has been modeled in *C. elegans*. The first model was established by overexpressing a huntingtin fragment with a 150CAG-repeat in sensory neurons of the worm in which the cytoplasmic aggregates of the protein increased with age and the neurons finally died through apoptosis [83]. Moreover, driving of the expression of 57 N-terminal residues of huntingtin in touch neurons resulted in touch sensitivity deficits of the worms [84].

The aforementioned models can give precious insights in the mechanisms underlying neurodegenerative diseases. The suitability of *C. elegans* for genetic screens gives great value to the "humanized" worm models for neurodegenerative diseases: new genes involved in these pathologies can be identified fast as well as their function [85]. Lastly, *C. elegans* mitochondrial mutants can be studied as a model of neurodegeneration as a result of mitochondrial deficiency as shown by the present and other studies [86].

Aim of the study

The aim of this study was to identify the mechanism or some of the molecular players connecting mitochondrial impairment to neuronal remodeling. The connection of these two is of high interest since neuronal remodeling occurs in neurodegenerative diseases where mitochondrial deficiencies have been shown to play an important role. Therefore, we wanted first to confirm that mitochondrial impairment in a simple model can interfere with the morphology of neuronal arborizations. We chose *C. elegans* due to its suitability for studies that include genetic approaches and its very well mapped nervous system. After confirming that the neuronal architecture of *C. elegans* is affected in animals having mitochondrial impairments due to genetic lesions, we aimed to identify the signaling pathway that regulates this phenomenon.

3. Materials & Methods

Note: All the solution recipes (Table 1), reagents (Table 2), plasticware/glassware (Table 5) and pieces of equipment (Table 6) mentioned in the methods below are listed in the respective tables at the end of this section. In addition, tables containing all the primer sequences (Table 4) and all the *C. elegans* strains (Table 3) used in this study are included.

3.1 Strain maintenance

- **3.1.1 Plate preparation and nematode culture**

  Reagents and equipment: Petri dishes (55 or 90 mm diameter), NGM, OP50 cultures, LB medium

  Method description: The NGM was prepared (see Buffers and Media Table) and autoclaved. While still in liquid form, it was poured into petri dishes of either 55 or 90 mm diameter. In case the plates were going to be used for treatments (with Vitamin C or AICAR) the substances were added before the medium was poured into the petri dishes. The plates were left for 2 days in room temperature to dry and to detect possible contaminations. Then, the plates were stored at 4-8ºC for up to 1 month, unless they contained Vitamin C or AICAR in which case the plates were used within 5 days after their preparation. Before its use, each plate was seeded with an OP50 bacterial lawn. OP50 is an *E. coli* strain which has a uracil auxotrophy and its growth is limited on NGM plates, thus forming a thin lawn which allows easy detection of the nematodes.

  A glycerol stock of OP50 was kept at all times at -80ºC and a fresh streaking was prepared every 2 weeks on an LB-agar plate and kept at 4ºC. An OP50 culture was prepared by adding one colony from the streaking plate in 200 mL LB medium in a conical flask and left for 6-8 hours at 37ºC under vigorous shaking. Then, 200 µL or 1 mL, for 55 mm and 90 mm plates respectively, were pipetted on each NGM plate and left to dry overnight at room temperature. The next day the plates had a dry and grown bacterial lawn ready for use. The rest of the bacterial culture was kept at 4ºC and refreshed every 3-4 days.

  Adult animals, larvae, thawed stocks or freshly bleached eggs (see below) were placed on the surface of NGM plates seeded with OP50 bacterial lawns. The animals were left to grow until the desired stage or population size was reached and they were used

for further experiments according to the respective needs. NGM plates containing starved populations were chunked, the chunks were placed on freshly seeded plates and the nematodes were left for 3-4 days to recover before starting new experiments.

- **3.1.2 Bleaching**

  Reagents and equipment: bleaching solution, M9 buffer, sterile distilled H_2O, Bunsen burner, stereomicroscope.

  Method description: The bleaching is conducted in order to synchronize a nematode culture or to clean contaminations. The bleaching solution dissolves the bodies of the nematodes whereas if the exposure is short enough, the eggs are left unharmed. Therefore, the culture intended for bleaching needs to contain gravid adult animals.
  Briefly, the animals were washed with H_2O and put into 1.5 mL eppendorf tubes. The animals were left to settle and were washed 3 times. 100 µL of the supernatant were left in the tube where 500 µL of bleaching solution were added. The tubes were vortexed for 4-5 minutes until the bodies of the adult nematodes were dissolved and not detectable under a stereomicroscope. Then the tubes were immediately centrifuged at 10,000 rpm for 1 minute and the excess bleaching solution was discarded and replaced by sterile M9 buffer close to a flame. This step was repeated 3 times and finally the egg pellet was resuspended in 100-200 µL of M9 buffer and distributed on freshly seeded NGM plates.

- **3.1.3 Long term storage (freezing)**

  Reagents and equipment: S buffer, freezing solution, 1.8 mL cryo tubes.

  Method description: *C. elegans* stocks can be prepared and stored at -80ºC or liquid nitrogen for several years. The nematodes that have the greatest possibility of recovering after freezing are of the L1 stage, if frozen when freshly starved. In this study, for every strain requiring a stock preparation we used 4-6 NGM 90 mm diameter plates that contained as many freshly starved L1 larvae as possible. The animals were washed with S buffer and put into a 15 mL falcon tube. The volume was adjusted at 7 mL, an equal volume of freezing solution was added, and the mixture was equally distributed in 8 1.8 mL cryo tubes. The tubes were stored at -80ºC. A

week later one of the vials was thawed and a successful freezing was confirmed if minimum 100 larvae survived one day after the thawing.

3.2 Ageing experiments

Reagents and equipment: 55mm diameter NGM plates freshly seeded with OP50, platinum wire pick, stereomicroscope.

Method description: A synchronized *C. elegans* cohort can be followed throughout its lifespan by selecting individuals and separating them from their progeny. Briefly, bleached eggs were placed on freshly seeded NGM plates. After 3 days 30-40 animals were selected and placed on 2-3 fresh NGM plates. These animals were separated from their progeny by transferring them every other day on new NGM plates. Censored animals (desiccated, with internal hatching or vulval protrusions) were excluded from this analysis. In this study we followed nematode cohorts for 10 days after the eggs hatched and imaged their neurons at 4, 6 and 10 days after their hatching.

3.3 Genotyping

- **3.3.1 Cross**

Reagents and equipment: 55mm diameter NGM plates seeded with a drop (~20 µL) of OP50 (mating plates), normally seeded 55mm diameter NGM plates.

Method description: The first step of a cross is the generation of males for one of the two participating strains. The males have a single X chromosome (XO) as compared to hermaphrodites that have two (XX). The generation of gametes lacking one X chromosome happens when the segregation of the two X chromosomes during meiosis is inhibited. In the laboratory, we mimic the conditions causing the lack of X chromosome segregation by exposing animals that are still developing their gonads to heat stress. For this reason, 3-4 L4 larvae from the selected strain were placed in 55 mm diameter NGM plates and incubated at 32ºC for 4 hours. After the incubation, the plates were moved to normal temperature (20ºC) while waiting for the L4s to develop and give progeny. In this generation some males were expected to be found. When the

males were obtained they were expanded so that the crosses could start. To maintain/expand the male population, nematodes with a high ratio of males/hermaphrodites were kept in the plates so that the chance of heterosexual mating is high.

In this study, when the males had reached a sufficient population, we placed 15-20 of them on a mating plate with 1 or 2 young adult hermaphrodites of the other strain of interest. The males were left with the hermaphrodites for 2 days and the progeny (F1) was picked with a platinum wire and singled out in separate NGM plates. The F1 animals were left to lay eggs for 2 days and then each animal was separately lysed and genotyped in order to find which one/ones carried the mutation/mutations of interest. The progeny of these F1 animals (F2) would undergo the same selection process. This set of steps was repeated for a number of generations (usually 4-6) until the desired genotype was obtained.

- **3.3.2 Polymerase chain reaction (PCR) and agarose gel electophoresis**

  Reagents and equipment: Lysis buffer, proteinase K (100 mg/mL), Taq polymerase, Taq polymerase buffer, dNTPs, PCR tubes, TBE buffer, agarose, agarose gel electrophoresis chambers, thermocycler.

  Method description: Briefly, PCR is used to amplify a particular DNA sequence. It requires thermal cycling, which consists of repeated cycles of heating and cooling for DNA melting and enzymatic replication. Primers containing sequences complementary to the target region and a DNA polymerase are necessary for a selective and repeated amplification. As the PCR progresses, the generated DNA is itself used as a template for replication, thereby promoting an exponential amplification of the template.

  In our study, firstly the worm lysate that would be used as a DNA template was obtained. As mentioned above, this came from a single worm. One animal was placed with the help of platinum wire and a stereomicroscope in a 0.2 mL PCR tube which contained 10 µL lysis buffer and 0.2 µL proteinase K. The tubes were placed in a thermocycler and incubated following the sequence: 1 hour at 65ºC (lysis), 10 minutes at 95ºC (proteinase K inactivation) and paused at 4ºC. At this point the lysates could be stored at -20ºC or immediately used for a PCR reaction.

Usually, the design of the primers used in each reaction is based on the nature of the mutations the crossed strains carry. For example, if the mutation is a deletion, the primers are designed accordingly so that they anneal either in the deleted part or in the regions flanking the deletion. In the first case the PCR will yield a product for the wild type but not the mutated allele, whereas in the second case the product for the wild allele will be longer compared to the one of the mutated allele. For all the primer sequences, see the Table 4 at the end of this section.

Each PCR reaction was set as follows:

- ✓ 2 µL worm lysate (DNA template)
- ✓ 0.3 µL forward primer (10µM)
- ✓ 0.3 µL reverse primer (10µM)
- ✓ 1.5 µL 10x Polymerase Taq buffer
- ✓ 1.5 µL dNTPs 2mM each
- ✓ 0.1 µL Taq Polymerase (5 U/µL)
- ✓ 9.3 µL H_2O

Total reaction volume: 15 µL

According to the number of samples that needed to be examined for a specific allele, one master mix was prepared containing all the reagents required for a PCR reaction, apart from the template. This master mix was then distributed among the tubes containing the DNA templates.

After the PCR reaction, the presence or size of the product needed to be assessed. For that purpose the reactions were loaded into agarose gels which were stained with ethidium bromide which intercalates into the major grooves of the DNA and fluoresces under UV light. The DNA products were separated by applying an electric field which makes the negatively charged molecules move according to their size. The PCR products could be detected with the help of a UV lamp and with a standard DNA ladder, their size was determined. In this study, since all of the PCR products were sized from 100 to 500 base pairs (see Table 4), the gels used were 1.5 % w/v and contained ethidium bromide at a final concentration 0.5 µg/mL. The gel electrophoresis was conducted at 120-140 mV and it lasted 30-40 minutes depending on the size of the gel.

3.4 Confocal microscopy

Reagents and equipment: mounting medium, microscope glass slides, coverslips, platinum wire pick, stereomicroscope and confocal microscope.

Method description: Properly staged nematodes were left to crawl on bacteria-free surface of an NGM plate for 5 minutes in order to remove the bacteria from their bodies. 10-15 animals were then picked with a platinum wire and left in a 15 µL drop of mounting medium on a glass slide. The mounted animals were gently covered with a 24x24 mm coverslip which was sealed with nail polish. The preparation was immediately taken for imaging and a new one was prepared every 20 minutes until the desired number of animals was imaged. The imaging was conducted using an inverted Zeiss LSM700 confocal microscope equipped with several objective lenses. For this study an oil-immersion 40x objective lens was used. The imaging conditions included the use of a 488 nm laser at 1-2% of its power capacity, a pinhole of 70 µm and the image resolution was 1024x1024 to maximize precision during analysis of the images.

3.5 Western Blotting

- **3.5.1 Protein extraction**

  Reagents and equipment: RIPA buffer supplemented with PhosSTOP (1 tablet/10 mL) and Protease Inhibitor Cocktail (1/2 tablet/10 mL), sterile distilled H_2O, ultrasonic disintegrator.

  Method description: The animals intended for western blotting were synchronized and collected on day 4. The animals were collected by washing the NGM plates with sterile distilled water and put into 1.5 mL eppendorf tubes. The nematodes were allowed to settle and washed 3 times in order to remove any remaining bacteria. After removing the supernatant of the last wash, the nematodes were resuspended in RIPA buffer supplemented as noted above. The amount of the added RIPA buffer varied from 80 to 150 µL according to the number of collected nematodes. The samples were kept on ice and sonicated with an ultrasonic disintegrator at medium amplitude for 10-15 seconds until no unsolved particles could be detected in the tube. The samples were then centrifuged at 14.000 rpm for 20 minutes at 4ºC. Finally, the supernatant was

transferred into a clean tube. The samples at this stage could be either quantified for their protein content (see below) or stored at -20ºC until further use.

- **3.5.2 Protein concentration determination (Bradford assay) and sample preparation**

  Reagents and equipment: Bio-Rad Protein Assay Dye Reagent Concentrate diluted 1:5, Albumin fraction V dissolved in H_2O at 1 mg/mL (BSA), laemmli buffer 4x, sterile distilled water, cuvettes, spectrophotometer.

  Method description: The principle of the Bradford assay is based on the fact that an acidic solution of the dye Coomassie Brilliant Blue G-250 can shift its absorbance maximum from 465 nm to 595 nm when bound to protein. Thus, measuring the absorbance of protein samples diluted in the dye at 595 nm gives a number proportional to the protein concentration of each sample.

  In this study, for each Bradford assay a standard curve was generated in order to define the relation of the absorbance and the protein concentration of standard samples before measuring the ones intended for gel electrophoresis. For that purpose a BSA solution of known concentration was used. For each sample and standard we used duplicates to overcome pipetting errors. For the standards, 2 to 16 µL of BSA were pipetted in eppendorf tubes, whereas for the protein samples we used 2 µL. 1 mL of the diluted dye was added in each tube and they were inverted several times for mixing. The tubes were incubated for 5 minutes at room temperature. Before starting the measurement the spectrophotometer was adjusted at 595 nm and blanked with a sample containing only dye. Then, starting from the standard samples, we measured the absorbance of each one at a spectrophotometer at 595 nm after transferring each sample into appropriate cuvettes. The absorbance of the standards versus their concentration was plotted and the resulting equation was used to calculate the concentration of every sample.

  After calculating the concentration of each sample, they were aliquoted as follows: x µL of protein sample which contained 20 µg of protein and x/3 µl laemmli 4x. If the volume difference between the aliquots was greater than 5 µL, 1x laemmli was added to bring all the samples to the same volume. The samples were then boiled at 95ºC for

5 minutes. At this point the samples could either be stored at -20ºC or used for SDS polyacrylamide gel electrophoresis immediately.

- **3.5.3 SDS polyacrylamide gel electrophoresis (SDS-PAGE) and gel transfer**

  Reagents and equipment: Upper buffer, lower buffer, APS, TEMED, running buffer, acrylamide, transfer buffer, nitrocellulose, filter paper, sterile distilled H_2O, protein marker, gel and transfer chambers.

  Method description: Polyacrylamide gel electrophoresis (PAGE) is a technique used to separate macromolecules according to their electrophoretic mobility. In this study SDS-PAGE was used for protein separation and the protein samples were treated with SDS in order to render them a negative charge. Therefore, the different proteins, when mobilized under an electrical field, get separated in the gel according to their size.
  Each gel consisted of two separately prepared gels; the stacking and the resolving gel. The purpose of the stacking gel is the concentration of the samples into tight bands before they enter the resolving gel. This is achieved through the almost neutral pH of the resolving gel (pH6.8) in which the Cl^- ions (from the Tris-HCl) and the neutrally charged form of glycine can migrate in certain manner forming a narrow zone of two migrating fronts. When this migrating zone passes through the sample well the proteins are concentrated into a narrow band between the two fronts of migrating ions. When the ion front reaches the resolving gel, due to its alkaline pH (pH8.8) the glycine gets negatively charged and migrates faster compared to the proteins. The proteins enter a gel with a higher acrylamide percentage, ergo smaller pores, and they can start moving and separating according to their size.
  Briefly, the resolving gel was prepared in a 50 mL falcon tube (recipe below) and immediately poured between two glassplates assembled on a gel holder according to the manufacturer's instructions. Approximately 2 cm from the top were left free for the stacking gel to be poured once the resolving gel was solid. The resolving gel was overlaid immediately after pouring with 1-2 mL of isopropanol to insure a flat surface. After 15-20 minutes, when the resolving gel had solidified, the stacking gel was prepared and similarly poured on top of the stacking gel after removing the isopropanol remains. A 10 well comb was immediately placed and left until the stacking gel was solid, to form the loading wells.

Resolving gel 12%:

- ✓ 20% v/v 30% acrylamide
- ✓ 25% v/v Lower buffer
- ✓ 1% v/v 10% APS
- ✓ 0.1% v/v TEMED

For each gel of 1.5 mm of thickness, 10 mL of resolving gel were prepared.

Stacking gel 6%:

- ✓ 40% v/v 30% acrylamide
- ✓ 25% v/v Upper buffer
- ✓ 1% v/v 10% APS
- ✓ 0.1% v/v TEMED

For each gel of 1.5 mm of thickness, 4 mL of stacking gel were prepared.

After 15-20 minutes, the combs were removed and the gels were placed inside an electrophoresis chamber according to the manufacturer's instructions. The chamber was filled with 1x Running buffer as well as the loading wells. The protein aliquots prepared in earlier steps were loaded in the wells. One well out of ten was always used for a protein marker. The gels were left to run at 120 V for approximately 1.5 hours. After that, the proteins in the gel were ready to get transferred.

The proteins were transferred from the gel to a nitrocellulose membrane, which served as a solid substrate, through tank blotting. In this case, the gel and the nitrocellulose membrane were stably assembled in a cassette by the use of filter paper and foam pads to ensure continuous contact between the two and at the same time access of the buffer everywhere in the assembly (see Schematic 1). Then, the cassette was assembled into a chamber according to manufacturer's instructions, the chamber was filled with 1x Transfer buffer and a cooling unit and the blotting was done at 400 mA for 1.5 hours. After that, the membrane was ready to use for immunoblotting.

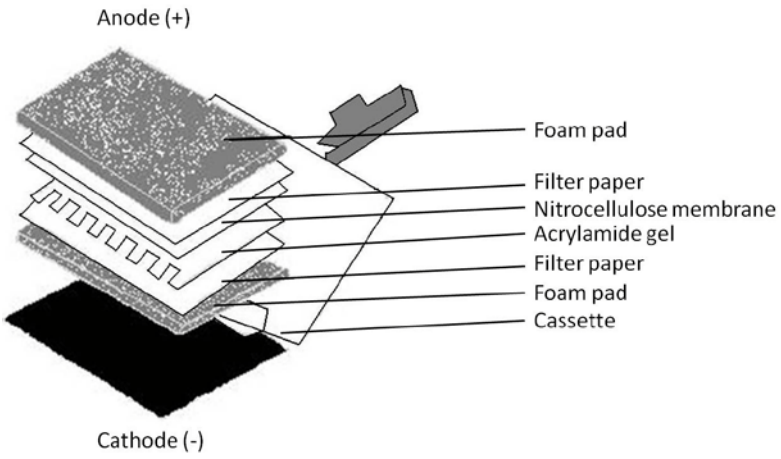

Schematic 1: The acrylamide gel and the nitrocellulose membrane were placed in the cassette as shown here. During the electrophoresis the proteins moved from the cathode to the anode thus attaching onto the solid substrate provided by the nitrocellulose.

- **3.5.4 Immunoblotting**

  Reagents and equipment: TBS-Tween 0.05%, blocking buffer, antibodies, ECL Western Blotting Substrate, tube roller, ChemiDoc^{TM} imaging system.

  Method description: Briefly, immunoblotting is based on the antibody-antigen recognition. After the proteins are fixed on nitrocellulose we use antibodies raised against a protein of interest. These antibodies are called primary and are being recognized by secondary antibodies which are raised in another species and recognize and bind onto heavy chains of the primary antibodies of the first species. In addition, the secondary antibodies are conjugated to an enzyme, namely horseradish peroxidase, which cleaves a chemiluminescent agent and the reaction product produces luminescence proportional to the amount of protein detected by the primary antibody.
  In this study, after the transfer was completed the nitrocellulose membranes were placed in 50 mL falcon tubes and blocked with blocking buffer for 1 hour at room temperature. This step was done on a tube roller at low speed. After the blocking step, the blocking buffer was removed and the primary antibody which was diluted 1:1000, apart from tubulin that was diluted 1:5000, in blocking buffer, was added in the tube containing the membrane. The incubation was done overnight at 4ºC at a low rolling speed. The next morning, the membranes were washed 3 times with TBS-Tween 0.05% and the secondary antibody was added which was in each case diluted 1:3000.

The secondary antibody incubation lasted 1 hour at room temperature and before developing, the membrane was washed 3 times with TBS-Tween 0.05%.

Before developing the membranes, each one was dried from the excessive TBS-Tween and covered with ECL for 1 minute. The membrane was then quickly placed between two pieces of transparent colorless plastic and put into a ChemiDoc™ imaging system for development. The exposure lasted 30 seconds to 4 minutes depending on the strength of the signal.

3.6 Neurite branch quantification

Required software: ZEN software by Zeiss

Method description: The ZEN software contains all the tools necessary for image processing and measurements. In our study, for every image the "Maximum Intensity Projection" option was firstly applied. This made the image analysis significantly faster since all the slices of a *z*-stack could be projected into one single image. Under the tab "Overlay" the ZEN software has a number of tools by which lines of high accuracy can be drawn on the region of interest while the option of showing the size of each line within the image provides a full panel of measurements in relatively short time. In our case, the "Open Bezier" tool was used in order to measure the distance between 2º branches and the length of the body region imaged every time. The same tool was used to measure the total length of 3º branches for Figure 2e.

3.7 Statistical analysis

Required software: Prism by GraphPad Software

Method description: In the case of comparing 2 groups, Student's *t*-test was used. When 3 or more groups were compared, one-way ANOVA was used. All the results were expressed in mean± standard error.

Table 1

Buffers/Media

Buffer/Medium name	Buffer/Medium recipe
Bleaching solution	1% NaClO, 0.5 N NaOH
Blocking buffer	5% w/v non-fat dried milk in TBS-Tween 0.05%
Freezing solution	S Buffer (see below), 30% glycerin (v/v) (autoclaved)
Reducing Laemmli buffer 4x	40% Glycerol, 250 mM Tris/HCl pH 6.8, 8% SDS, 0.04% bromophenol blue, 20% beta-mercaptoethanol
LB medium	2% w/v of powder microbial growth medium (SIGMA)
LB agar	1.5% w/v agar in LB medium
Lower buffer	1.5 M Tris-base, 0.4% SDS, pH 8.8
Lysis buffer	50 mM KCl, 10 mM Tris-HCl (pH 8.1), 2.5 mM $MgCl_2$ (autoclaved)
Mounting medium	30% w/v polyethylene glycol 8000 in 25% v/v glycerol
M9 buffer	22 mM KH_2PO_4, 42 mM Na_2HPO_4, 85 mM NaCl, 1 mM $MgSO_4$
Nematode growth medium (NGM)	50 mM NaCl, 1.7% w/v agar, 0.25% w/v peptone (autoclaved and when at ~55ºC the following were added:) 1 mM $CaCl_2$, 5 µg/mL cholesterol diluted in EtOH, 1 mM $MgSO_4$, 25 mM KPO_4
PCR loading dye 10x	100 mM EDTA pH 8.0, 1% w/v SDS, 50% v/v glycerol, 0.1% w/v bromophenol blue
Running buffer 10x	250 mM Tris 1.92 M glycine 1% SDS

S buffer	6.45 mM K_2HPO4, 43.55 mM KH_2PO4 0,1 M NaCl (autoclaved)
Transfer Buffer 10x	250 mM Tris 1.92 M glycine (used 1x with 20% methanol)
Tris-buffered saline (TBS) 10x	153 mM Tris.HCl, 1.4 M NaCl, pH 7.4
Upper buffer	1M Tris-base, 0,4% SDS, pH 6.8

* The chemicals were purchased from Applichem, Roth, SIGMA and VWR

Table 2

Reagents

Reagent	Company
agarose	SIGMA
AICAR (5-Aminoimidazole-4-carboxamide ribonucleotide)	Toronto Research Chemicals Inc.
anti P-AMPK (T172)	Cell Signaling
anti-tubulin	SIGMA
APS (Ammonium persulfate)	SIGMA
Albumin Fraction V	Roth
Bio-Rad protein assay	Bio-Rad
DNA ladder-100bp	Applichem
dNTPs	Life Technologies
ethidium bromide	Applichem
Escherichia coli OP50	Hengartner Lab
filter paper	Bio-Rad
HRP-conjugated anti-mouse secondary antibody	Thermo Fisher Scientific
HRP-conjugated anti-rabbit secondary antibody	Thermo Fisher Scientific
PhosSTOP Tablets	Roche
Pierce ECL Western Blotting Substrate	Thermo Scientific
Protease Inhibitor Cocktail Tablets	Roche

proteinase K	Applichem
Precision Plus Protein™ All Blue Standards	Bio-Rad
RIPA buffer	SIGMA
Taq Polymerase (5 U/µL)	Life Technologies
TEMED (Tetramethylethylenediamine)	Merck
Tris/Borate/EDTA (TBE) buffer	Applichem
Tween20	Calbiochem
Vitamin C	SIGMA
Whatman nitrocellulose	GE Healthcare Life Sciences
10X PCR buffer	Life Technologies
30% (w/v) acrylamide/methylene bisacrylamide solution (37.5:1 ratio)	National Diagnostics

Table 3

C. elegans Strains

Strain name	Genotype	Source
OH1422	*otIs138* [*ser-2prom3::gfp; rol-6*]	CGC
SK4005	*zdIs5* [*mec-4p::gfp; lin-15(+) (pSK1)*]	CGC
nuo-6; otls138	*nuo-6*(*qm200*)*I*; *otIs138* [*ser-2prom3*::*gfp*; *rol-6*]	Hekimi Lab
BAN-54	*gas-1*(*fc21*)X; *otIs138* [*ser-2prom3*::*gfp*; *rol-6*]	cross
BAN-73	*daf-2*(*e1370*)*III*; *otIs138* [*ser-2prom3*::*gfp*; *rol-6*]	cross
BAN-74	*aak-2*(*ok524*)*X*; *otIs138* [*ser-2prom3*::*gfp*; *rol-6*]	cross
BAN-75	*daf-2*(*e1370*)*III*; *gas-1*(*fc21*)*X*; *otIs138* [*ser-2prom3*::*gfp*; *rol-6*]	cross
BAN-83	*gas-1*(*fc21*)*X*; *aak-2*(*ok524*)*X*; *otIs138* [*ser-2prom3*::*gfp*; *rol-6*]	cross
BAN-102	*gas-1*(*fc21*)*X*; *zdIs5* [*mec-4*::*gfp*; *lin-15*(+) (*pSK1*)]	cross
BAN-105	*age-1*(*hx546*)*II; otIs138* [*ser-2prom3*::*gfp*; *rol-6*]	cross
BAN-117	*age-1*(*hx546*)*II; gas-1*(*fc21*)*X; otIs138* [*ser-2prom3*::*gfp*; *rol-6*]	cross

Table 4: Primers

gene	allele	Forward primer (5‘->3‘)	Reverse primer (5‘->3‘)	Annealing temperature (°C)	Amplicon size (bp)
aak-2	wild type	agtcatcagtacaccttctgacattttca	agttgttgtgtctaatcttgttcaattactt	65	511
aak-2	*ok524*	agtcatcagtacaccttctgacattttca	agttgttgtgtctaatcttgttcaattactt	65	103
age-1	wild type	acccagtttgtacacaggatccagtag	gaatatcgccgtatctcacttctgatgg	65	231
age-1	*hx546*	acccagtttgtacacaggatccagtaa	gaatatcgccgtatctcacttctgatgg	65	231
clk-1	wild type	agatgtgggatgaggagaaagaa	cagtatcatgatgatgaagcgc	59	444
clk-1	*e2519*	agatgtgggatgaggagaaagaa	ccagtatcatgatgatgaagcgt	59	444
daf-2	wild type	aacacctcatcattactcaaaccaatatatag	ggaagctaatattatgaagaactttaagactaacttta	57.5	500
daf-2	*e1370*	caacacctcatcattactcaaaccaatatataa	ggaagctaatattatgaagaactttaagactaacttta	57.5	500
gas-1	wild type	atacttcgatcgtctcgattacgtct	ctgacacaagtccgatgtcaatagtac	58	420
gas-1	*fc21*	atacttcgatcgtctcgattacgtct	ctgacacaagtccgatgtcaatagtat	58	420
isp-1	wild type	caggagaaaaaagactgcataccaattag	gtcaaactatcgtcgtgattctacaaaga	62	525
isp-1	*qm150*	caggagaaaaaagactgcataccaattaa	gtcaaactatcgtcgtgattctacaaaga	62	525
nuo-6	wild type	atgtagaagagagcgaaaacggtac	tgataacatttgcgttgatgaaca	60	428
nuo-6	*qm200*	atgtagaagagagcgaaaacggtat	tgataacatttgcgttgatgaaca	60	428

Table 5

Plasticware & Glassware

Type of plasticware/glassware	Company
eppendorf tubes 1.5 mL/2 mL	eppendorf
falcon tubes 15 mL/50 mL	BD Falcon
strippetes 5 mL/ 10 mL/ 25 mL/ 50 mL	Costar
pipette tips 10 µl/ 200 µl/ 1000 µl	VWR
petri dishes 55 mm/90 mm diameter	Nerbeplus
0.2 mL PCR tubes	Nerbeplus
glass slides	Th. Geyer
coverslips (24x24mm)	Menzel-Glaesser
conical flasks /glass bottles/beakers	Schott/VWR
cuvettes	VWR
cryo tubes	Thermo Scientific
glassplates for acrylamide gels	Bio-Rad
gel holders and gel combs	Bio-Rad

Table 6

Equipment

Type of equipment	Company
bacterial incubator shaker	Stuart
Bunsen burner	WLD-TEC
chambers for gel electrophoresis and transfer	Bio-Rad
ChemiDoc™ imaging system	Bio-Rad
confocal microscope	Zeiss
hot plate	Grant
nematode/bacterial incubators	Binder
platinum wire 0.2 mm (32 gauge)	Neo Lab
power supplies for electrophoresis	VWR
spectrophotometer	eppendorf

stereomicroscope	Leica M80
stereomicroscope lamp	KL1500 LCD
thermocycler	Bio-Rad/Biometra
tube roller	NeoLab
ultrasonic disintegrator	MSE
UV lamp for agarose gel imaging	Syngene

4. Results

4.1 Generation of a *C. elegans* model for *in vivo* analysis of neuronal remodeling

In order to study the effects of mitochondrial dysfunction in neuronal architecture, we sought to find a model which would allow us fast imaging of its nervous system and flexibility in order to follow a genetic approach. These criteria are both fulfilled by the nematode *C. elegans*. *C. elegans* has a very well mapped nervous system and the animal's transparency allows live imaging of its nervous system with great speed. *C. elegans* is also suitable for genetics since obtaining new mutants via crossing can be done in short time [44]. In addition, obtaining transgenic strains that carry an array which leads the expression of a fluorescent protein in a group or a single neuron is simple: such strains can be obtained by the *Caenorhabditis* Genetics Center (CGC) or generated in house by generating extrachromosomal arrays via the microinjection method [56].

After selecting the model organism, we tried to indentify a neuron which could give an easy readout regarding neuronal architecture and remodeling. Although most of the *C. elegans* neurons are structurally simple and have unbranched projections [57], two pairs of neurons, the FLPs and the PVDs, have complex dendritic branches. The PVDs are mechanosensory neurons that have an extensive elaborate branching which envelops almost the entire body of the adult animal and its pattern is consistent between different individuals (Figure 1a) [57, 69]. The dendritic arborizations of these neurons comprise of repetitive structural units which resemble menorahs, hence their name. Overall, we started our study by selecting the PVD neurons as a model that would allow us to assess easily differences in neuronal architecture.

In order to visualize the PVDs we selected a transgenic *C. elegans* strain, namely OH1422, which carries an integrated transgene (*ser-2prom3::gfp*) driving the expression of GFP under the promoter 3 of *ser-2* (serotonin/octopamine receptor) [87]. This results into GFP expression in the PVDs, and two other mechanosensory neurons the OLLs and the PDEs. Since the PDE and the OLLs do not interfere with the branching pattern of the PVD, imaging of the latter was easily performed.

The stage we selected for imaging was day 4 after hatching which corresponds to the first day of adulthood (animals capable of laying eggs) when the animals are kept at 20ºC (apart from *nuo-6* mutants that need 7 days to molt into adults-see below). At this stage the PVDs are fully developed and therefore that is the stage we selected for imaging. As previously mentioned, the PVDs envelop the entire body of the adult worm. Therefore, in order to

accelerate our experiments both in terms of image acquisition and analysis, we focused on the posterior area of the body which was defined by the position the neuronal cell body to the end of the tail (Figure 1a). This area has the advantages of reduced interference of the eggs carried by adult animals with the imaging process, as well as reduced endogenous fluorescence which is redundant due to granules in the intestine or accumulated lipid particles in more anterior areas of the body. In addition, this part of the neuron represents more than 1/3 of the entire dendritic arborization, thus rendering the captions we studied representative of the organization of the entire neuron.

Nextly, we identified which were the traits of the PVD neuron we could measure and eventually use as readouts. Indeed, as indicated by our results, the number of 2º branches, the distance between them as well the same values for the 3º branches proved to be morphological properties of the neuron and are consistently altered under specific conditions (Figure 1b). Finally, for the needs of a certain experiment we used as readout the total length of 3º branch for the menorahs present in the area or interest (Figure 2e, see text for more information).

Overall, in the first phase of our study we established an *in vivo* model which would allow us to monitor easily and precisely neuronal remodeling and a great number of manipulations including the application of a genetic approach.

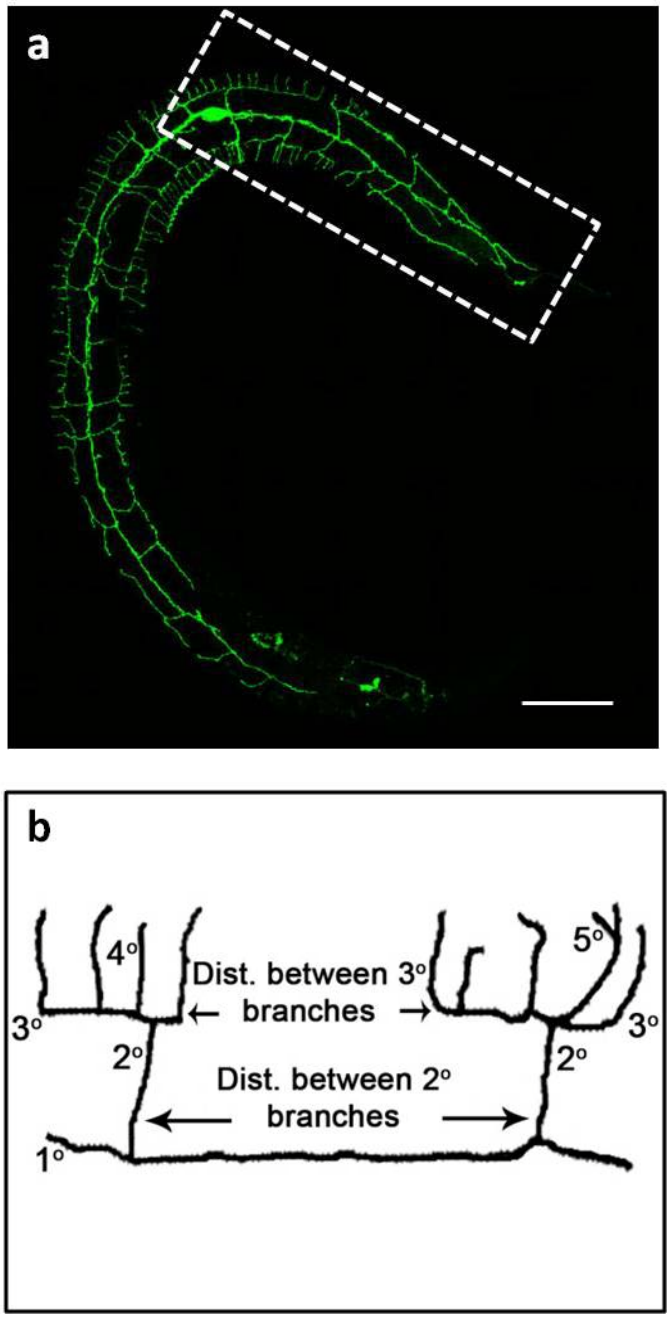

Figure 1: Establishment of an *in vivo* model to monitor neuronal remodeling. **a)** PVD neuron of a young adult animal (day 4). The dashed rectangle indicates the area of interest. Scale bar represents 50 µm. **b)** Schematic of part of the PVD neuron with indications of the variable traits we measured in this study.

4.2 OXPHOS impairment alters dendritic arborization in *C. elegans* sensory neurons

In order to study the effect of mitochondrial deficiency on the morphology of *C. elegans* neurons, we selected a mitochondrial mutant, namely *gas-1(fc21). gas-1* mutants are known to have altered sensitivity to volatile anesthetics, fecundity and reduced lifespan [88]. The *gas-1* gene encodes for a 49 kDa iron protein subunit of the mitochondrial Complex I. GAS-1 is widely expressed in the nematode neuromuscular system [89]. Animals carrying the *fc21* allele have reduced Complex I enzymatic activities as shown by measurements of oxidative phosphorylation and electron transport [89].

Indeed, analysis of the neuronal morphology of *gas-1* mutant animals carrying the integrated transgene *ser-2prom3::gfp* which drives *gfp* expression in the PVD neuron, showed altered dendritic pattern compared to wild type animals (Figure 2a). Specifically, *gas-1* animals had significantly more 2º branches than wild type animals in the same body region (Figure 2b). All our measurements were normalized to the length of the measured area in order to exclude the detection of differences due to differences in body size. In order to confirm the increased density of dendritic arbors in *gas-1* mutants, we also measured the distance between the 2º and 3º branches (Figure 2c-d). In agreement with our previous observation, the 2º branches occurred with almost a double frequency in *gas-1* mutants compared to wild type animals. Thus, our analysis suggests that Complex I impairment promotes branching. In addition, the total length of 3º branches is not affected in *gas-1* mutants (Figure 2e) -a fact that indicates an altered neuronal architecture with each menorah covering a smaller receptive field in these mutants.

After examining the phenotype of *gas-1* mutant animals, we wanted to determine whether it occurred specifically in this strain or other mutations causing OXPHOS impairment could have the same effect. To that end, we examined the neuronal morphology of a mutant strain overexpressing the transgene *ser-2prom3::gfp,* namely *nuo-6*(*qm200*). *nuo-6* encodes for the NDUFB4/B15 subunit of complex I [90]. Mutants carrying the *qm200* allele have been shown to have increased longevity -an effect caused by elevated levels of superoxide produced by their mitochondria [91]. In line with our evidence in *gas-1* mutants, *nuo-6* mutant nematodes exhibited significantly increased branching as demonstrated by the increased number of 2º branches and their increased density (Figure 2f-g).

Since animals carrying OXPHOS defects exhibit enhanced oxidative stress [90, 92] we wondered if treatment of *gas-1* mutant animals with an anti-oxidant would ameliorate the phenotype. As shown in Figure 2h, treatment of *gas-1* mutant nematodes with the antioxidant Vitamin C [93] did not rescue the phenotypic anomaly. This is in accordance with existing evidence showing that treatment with oxidants such as paraquat and hydrogen peroxide, did not affect the branching of certain neurons in *C. elegans* in a manner similar to OXPHOS mutants [62].

In summary, OXPHOS impairment alters dendritic morphology in the PVD neuron and this effect is independent of the mutation causing the OXPHOS impairment and uncoupled from increased oxidative stress.

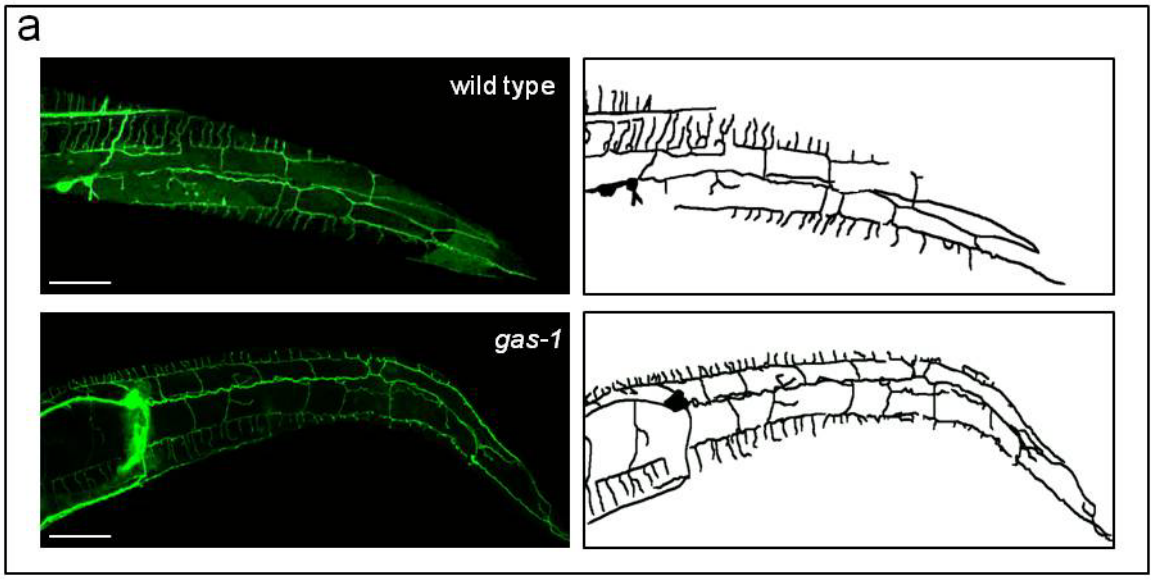
a
wild type
gas-1

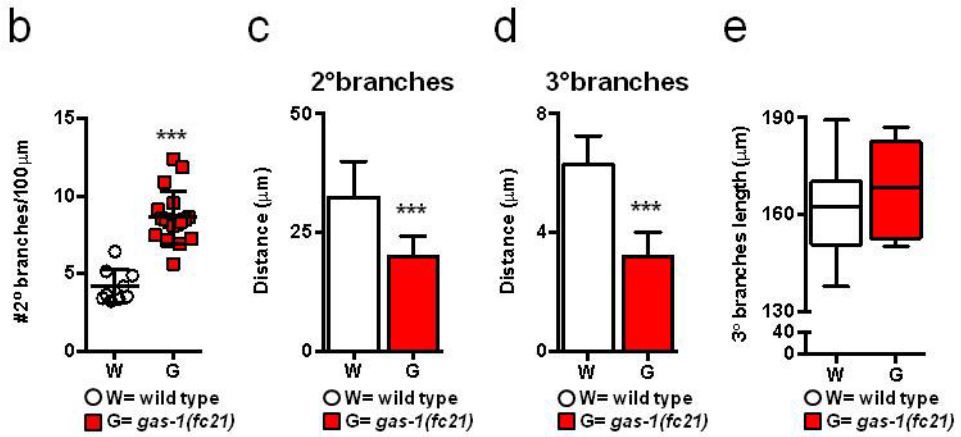
b
#2° branches/100 µm
***
W
G
W= wild type
G= gas-1(fc21)
c
2°branches
Distance (µm)
***
W= wild type
G= gas-1(fc21)
d
3°branches
Distance (µm)
***
W= wild type
G= gas-1(fc21)
e
3° branches length (µm)
W= wild type
G= gas-1(fc21)

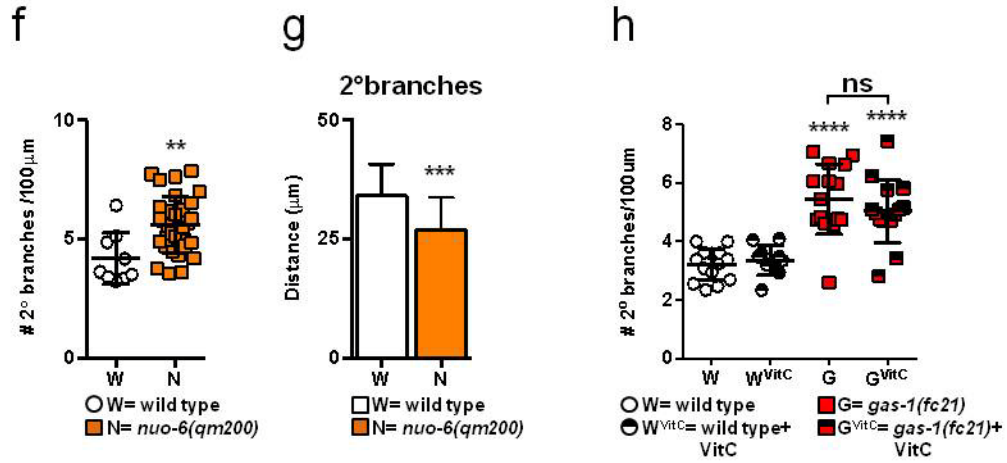
f
2° branches /100 µm
**
W
N
W= wild type
N= nuo-6(qm200)
g
2°branches
Distance (µm)
***
W= wild type
N= nuo-6(qm200)
h
ns
****
****
2° branches/100 um
W
W^VitC
G
G^VitC
W= wild type
G= gas-1(fc21)
W^VitC= wild type+ VitC
G^VitC= gas-1(fc21)+ VitC

Figure 2: Mitochondrial complex I deficiency results in increase of branching of *C. elegans* sensory neurons. **a)** Representative confocal images (left panel) and their schematic tracing (right panel) of wild type (W) and *gas-1(fc21)* mutant nematodes overexpressing the *ser-2prom3::gfp* transgene. Scale bars represent 25 µm. **b)** Quantification of 2º branches normalized to body length in wild type and *gas-1* mutant nematodes. **c)** Quantification of the distance between neighboring 2º branches in wild type and *gas-1* mutant animals. **d)** Quantification of the distance between neighboring 3º branches in wild type and *gas-1* animals. **e)** Quantification of the total length of 3º branches in wild type animals and *gas-1* mutants. **f)** Quantification of 2º branches normalized to body length in wild type and *nuo-6(qm200)* mutant nematodes. **g)** Quantification of the distance between neighboring 2º branches in wild type and *nuo-6* animals. **h)** Quantification of 2º branches normalized to body length in untreated and treated with 1 mM Vitamin C wild type and *gas-1* mutant nematodes. ****$P<0.0001$, ***$P=0.0001$, **$P<0.001$, one-way ANOVA (panel H) or Student's *t*-test; $n=3$ for each set of experiments.

4.3 Neuronal remodeling due to OXPHOS impairment is not cell-type specific

Based on our analysis, it is clear that OXPHOS impairment affects the architecture of the dendrites of the PVD neurons in *C. elegans*. What we wondered next was whether this effect is cell-type specific.

To that end we examined the morphology of a pair of light touch receptor neurons, the PLMs. These neurons have their cell bodies located in the tail and have a single process that projects anteriorly (Figure 3a). We specifically used a strain that overexpresses the integrated *mec-4p::gfp* transgene [94] and imaged the PLM neurons both in wild type and *gas-1* mutant animals. Our analysis revealed that while wild type animals rarely have ectopic structures on their PLM projections, *gas-1* mutant nematodes of the same stage demonstrated almost a two-fold increase in extra protrusions (Figure 3b).

In conclusion, the alterations in neuronal morphology due to OXPHOS impairment occur in *C. elegans* neurons in a cell-type independent manner.

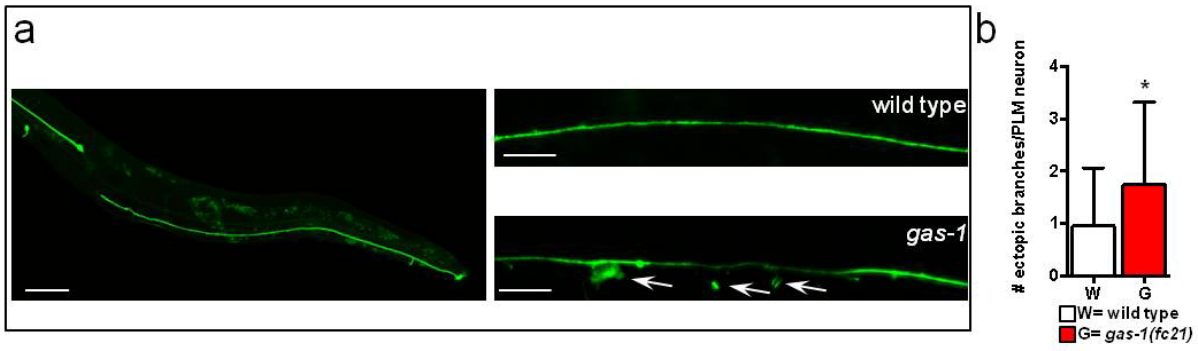

Figure 3: OXPHOS impairment affects the morphology of neurons in a non-cell type specific manner. **a)** Representative confocal image of a wild type animal (left panel) overexpressing the *mec-4p::gfp* transgene. Scale bar represents 50 µm. Representative confocal images (right panel) of a part of the PLM neuron of a wild type animal and a *gas-1* mutant nematode overexpressing the *mec-4p::gfp* transgene. The arrows indicate the ectopic processes. Scale bars represent 10 µm. **b)** Quantification of ectopic outgrowths in PLM neurons in wild type (W) and *gas-1* (G) mutants. *P<0.05, Student's t-test; n=3.

4.4 AMPK activity regulates dendritic branching

Nextly, we wondered which are the molecules that mediate excessive branching due to OXPHOS defects in nematodes. We considered as potential candidates molecules participating in signaling pathways that get activated due to energy deprivation as a consequence of OXPHOS impairment. AMP-activated protein kinase (AMPK) is a promising candidate since it is an energy sensor involved in many catabolic processes engaged during stress, including conditions of altered mitochondrial respiration [95, 96]. Specifically, decreased energy levels promote the binding of AMP to AMPK. This causes an allosteric activation that allows the phosphorylation or Thr172 in the alpha-kinase domain by upstream kinases like LKB1 or CaMKKbeta [97].

In *C. elegans aak-1* and *aak-2* encode two homologs of the alpha-catalytic subunit of the human AMPK, with AAK-2 participating in stress-response signaling pathways due to energy deprivation [98, 99]. We assessed the phosphorylation levels of *C. elegans* AMPK via western blot and observed significantly increased levels of phosphorylated AMPK in homogenates of *gas-1* animals compared to wild type (Figure 4a). As shown by the immunoblot, the lack of signal for *aak-2*-null mutant animals indicates that AAK-2 is the main phosphorylated AMPK (Figure 4a).

Considering the levels of AMPK phosphorylation under OXPHOS impairment conditions, we wanted to assess the role of AMPK in the excess branching observed in *gas-1* mutant nematodes. For that purpose we generated a double mutant strain *gas-1; aak-2* overexpressing the PVD fluorescent reporter. Analysis of the neuronal morphology of these double mutant nematodes revealed that the number of menorahs, 2º branches as well as the distance between them had no significant difference with their wild type counterparts (Figure 4b-d). This suggests that AAK-2/AMPK is required to induce branching due to OXPHOS deficiency.

On the basis of these observations, we hypothesized that overactivation of AAK-2/AMPK would mimic the conditions of OXPHOS impairment and lead to a similar enhancement of dendritic branching. In order to confirm our hypothesis, we treated nematodes with 5-amino-imidazole-carboxamide riboside (AICAR). AICAR is an AMP mimetic that binds and activates AMPK and has been suggested as a treatment for mitochondrial disorders [100]. In accordance with our previous results, treatment with AICAR induced dendritic branching in wild type nematodes but it had no effect on *gas-1* mutants (Figure 4f). The specificity of AICAR was confirmed via western blot where we observed an increase in the levels of

phosphorylated AMPK for wild type animals and detected no phosphorylated AMPK for *aak-2*-null mutants (Figure 4e). Additionally, the lack of effect of AICAR on the number of dendritic branches of *aak-2*-null mutants further confirmed the specificity of the compound (Figure 4g).

Overall, our observations suggest that the enhanced dendritic branching associated with mitochondrial OXPHOS deficiency in nematodes is mediated by the phosphorylated AAK-2/AMPK.

4.5 PI3K/AGE-1 acts downstream of AMPK to regulate dendritic arborization

In search of molecular actors that can act downstream of AMPK and be involved in dendritic branching, we examined the role of phosphoinositide 3-kinase (PI3K). This protein belongs to a family of intracellular signal transducer enzymes capable of phosphorylating the 3 position hydroxyl group of the inositol ring of phosphatidylinositol. In addition, PI3K has been involved in axonal neurite growth during polarization of mammalian hippocampal neurons localizing to the tip of newly specified axons [101, 102]. Interestingly, activated AMPK can disrupt the association of PI3K with the kinesin Kif5 and consequently prevent the targeting of PI3K to the axonal tip. By extension, this inhibits neuronal polarization and axon growth [103]. Thus, we sought to investigate if PI3K is involved in the phenotype of excessive branching in our OXPHOS mutants.

In *C. elegans, age-1* encodes for the homolog the *p110* catalytic subunit of the mammalian PI3K [104]. To determine if PI3K has a role in dendritic outgrowth, we generated *C. elegans* strains carrying a loss-of-function allele (*hx546*) of the *age-1* gene. In line with our working hypothesis, *age-1* loss-of-function suppressed completely the increased dendritic branches induced by OXPHOS impairment as shown by the analysis of the neuronal morphology conducted on *age-1; gas-1* double mutants (Figure 4b-c).

Finally, we wanted to determine whether AAK-2 acts upstream of AGE-1. To that direction we treated *age-1* mutant animals with AICAR. We hypothesized that if AAK-2/AMPK acts upstream of AGE-1/PI3K, AICAR treatment would not promote dendritic branching in these mutants. In support of our hypothesis, *age-1*-loss-of-function suppressed significantly the effect of AICAR (Figure 4h).

Collectively, our findings indicate that AGE-1/PI3K is involved in the formation of excessive dendritic branches induced by AAK-2/AMPK hyperphosphorylation and it specifically acts downstream of the latter.

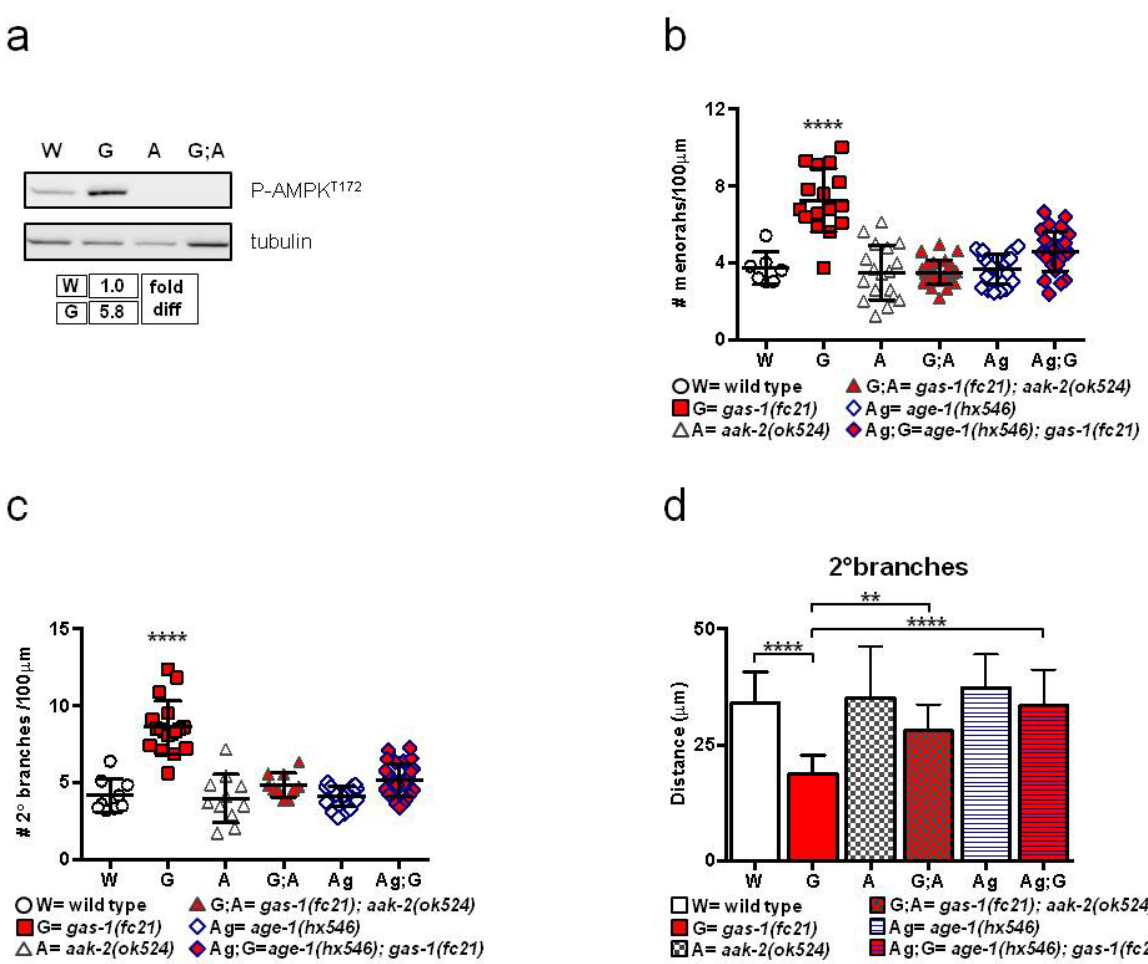
a
W G A G;A
P-AMPK^{T172}
tubulin
W 1.0
G 5.8
fold diff
b
# menorahs/100µm
W= wild type
G= gas-1(fc21)
A= aak-2(ok524)
G;A= gas-1(fc21); aak-2(ok524)
Ag= age-1(hx546)
Ag;G=age-1(hx546); gas-1(fc21)
c
2° branches /100µm
d
2°branches
Distance (µm)
e
W G Ag A
AICAR
P-AMPK^{T172}
tubulin
+AICAR
W 1.0
W 1.5
G >5
G >5
Ag 1.7
Ag >5
fold diff
f
#2° branches/100µm
ns
W= wild type
W^{AIC}= wild type+ AICAR
G= gas-1(fc21)
G^{AIC}= gas-1(fc21)+ AICAR
g
# 2° branches/100 µm
A= aak-2(ok524)
A^{AIC}= aak-2(ok524)+ AICAR
h
# 2° branches/100um
Ag= age-1(hx546)
Ag^{AIC}=age-1(hx546)+ AICAR

Figure 4: AMPK regulates dendritic branching in nematodes with impaired OXPHOS through PI3K: **a)** Western blot showing the protein levels of phosphorylated AMPK (T172) (and tubulin as a loading control) in extracts from wild type (W), *gas-1* (G), *aak-2* (A) and *gas-1; aak-2* (G;A) mutant nematodes (*n*=1). **b-c)** Quantification of number of menorahs (b) and number of 2º branches (c) normalized to the body length in wild type, *gas-1*, *aak-2*, *gas-1; aak-2*, *age-1* and *age-1; gas-1* mutants. **d)** Quantification of the distance between neighboring 2º branches in wild type, *gas-1*, *aak-2*, *gas-1; aak-2*, *age-1* and *age-1; gas-1* mutants. **e)** Western blot showing the protein levels of phosphorylated AMPK (T172) (and tubulin as loading control) for untreated and treated with 1 mM AICAR wild type (W), *gas-1* (G) *age-1* (Ag) and *aak-2* (A) mutant nematodes (*n*=1). **f)** Number of 2º branches normalized to the body length in wild type and *gas-1* mutant nematodes untreated or treated with 1 mM AICAR. **g)** Number of normalized 2º branches in *aak-2* mutant animals untreated or treated with 1 mM AICAR. **h)** Number of 2º branches normalized to the body length in wild type and *age-1* mutant animals untreated or treated with 1 mM AICAR. ****P<0.0001, ***P<0.001, **P<0.01, *P<0.05, one-way ANOVA, *n*=3 (unless otherwise indicated) for each set of experiments, 15-30 animals per condition were analyzed in total.

4.6 OXPHOS impairment-induced dendritic branching is uncoupled from accelerated aging

Age-related increase of dendritic branching has been previously reported in *C. elegans*. Specifically, it was shown that sensory neurons of aged animals had higher probability of displaying newly formed ectopic outgrowths compared to their younger counterparts [62, 63]. Since our study revealed a similar effect due to OXPHOS impairment, we sought to determine whether the observed phenotype was linked to accelerated ageing of the short-lived OXPHOS mutants.

For this purpose, we assessed the morphology of the PVD neuron in the long lived *daf-2* mutant animals carrying the *ser-2prom3::gfp* integrated transgene. The *daf-2* gene encodes for the sole insulin/IGF-1 receptor in *C. elegans* and mutants carrying the hypomorphic allele *e1370* display prolonged lifespan [105]. We demonstrated that *daf-2*(*e1370*) mutant nematodes have increased phosphorylation levels of AMPK as shown in the immunoblot of Figure 5a. Assessment of their neuronal morphology revealed that *daf-2* mutants have significantly increased 2º branches as well as decreased distance between them (Figure 5b-c). Importantly, *daf-2; gas-1* double mutants which live longer than the individual single mutants (Troulinaki *et al*, manuscript in preparation), also have significantly increased number of 2º branches and decreased distances between them (Figure 5b-c).

In order to further support our findings, we assessed the morphological alterations that occur in the PVD neuron due to ageing. As shown in Figures 5d-f, the morphological alterations that present on day 6 and deteriorate by day 10 are not similar to the dendritic alterations we report in mutant strains having OXPHOS impairments. Six days after hatching the PVD displays a significant increase of randomly distributed ectopic outgrowths and loss of distinction between neighboring menorahs (Figure 5f). This phenotype is more pronounced as the animals age further. Indeed, 10 days after hatching the loss of distinction between neighboring menorahs is significantly increased (Figure 5e). This type of structural alteration differs from the dendritic alterations we found in *gas-1* or *nuo-6* mutants and it supports even further the uncoupling of OXPHOS impairment-induced dendritic branching from accelerated aging.

Overall our findings indicate that alterations of the ageing pace or lifespan are not contributing factors to the excessive branching due to OXPHOS compromise. This is in line with our observation that *nuo-6* mutants that have OXPHOS impairment but live longer compared to wild type animals, still display increased number of dendritic branches.

a

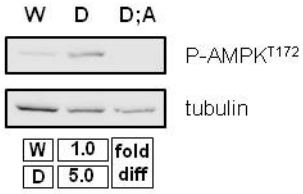
W D D;A
P-AMPK^{T172}
tubulin
W 1.0 fold
D 5.0 diff

b

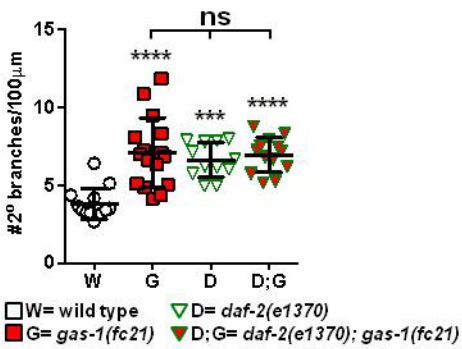
#2° branches/100µm
ns
****
***
****
W G D D;G
W= wild type
G= gas-1(fc21)
D= daf-2(e1370)
D;G= daf-2(e1370); gas-1(fc21)

c

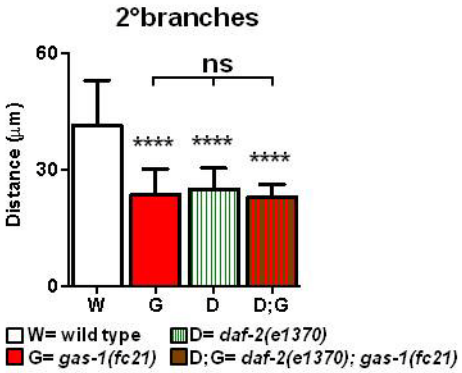
2°branches
Distance (µm)
ns
****
****
****
W G D D;G
W= wild type
G= gas-1(fc21)
D= daf-2(e1370)
D;G= daf-2(e1370); gas-1(fc21)

d

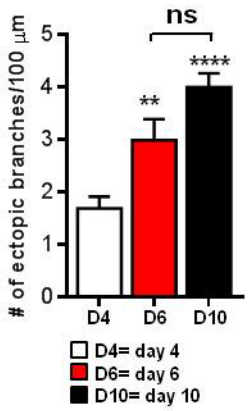
# of ectopic branches/100 µm
ns
**
****
D4 D6 D10
D4= day 4
D6= day 6
D10= day 10

e

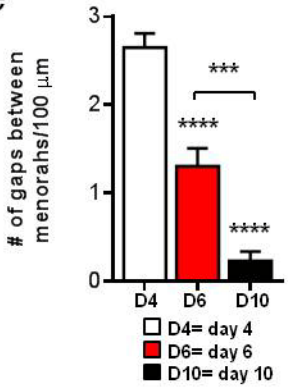
# of gaps between menorahs/100 µm
***
****
****
D4 D6 D10
D4= day 4
D6= day 6
D10= day 10

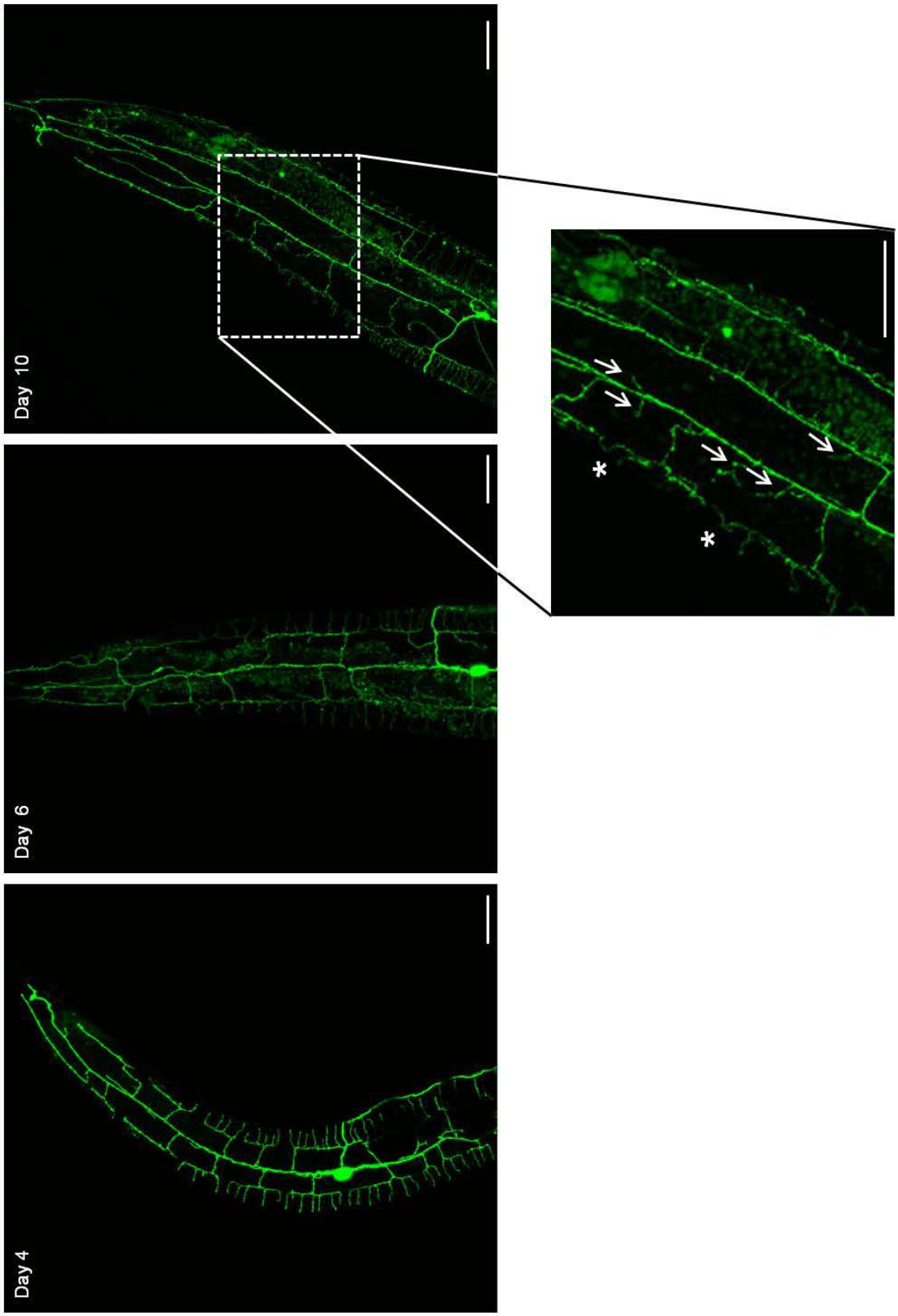
f
Day 4
Day 6
Day 10

Figure 5: OXPHOS impairment-induced dendritic branching is uncoupled from accelerated aging. **a)** Western blot of phosphorylated AMPK (T172) and tubulin in samples from wild type (W), *daf-2* (D) and *daf-2; aak-2* (D;A) mutant nematodes (*n*=1). **b)** Measurement of the number of 2º branches normalized to the body length in wild type, *gas-1*, *daf-2* and *daf-2; gas-1* mutant nematodes. **c)** Quantification of the distance between 2º branches in wild type, *gas-1*, *daf-2* and *daf-2; gas-1* mutant nematodes. **d,e)** Measurement of ectopic branches of 4, 6 and 10 days old wild type animals normalized to the body length (d) and quantification of the gaps separating neighboring menorahs (e) (n=2). **f)** Representative images of the PVD neuron in 4, 6 and 10 days old wild type animals. The asterisks in the insert indicate the contact between neighboring menorahs and the arrows indicate ectopic branches. Scale bars of the images and of the insert represent 25 µm. ****P<0.0001, ***P<0.001, **P<0.01, ns= not significant, one-way ANOVA, n=3 (unless otherwise indicated) for each set of experiments and 15-20 animals per condition were analyzed in total.

5. Discussion

Multiple lines of evidence implicate mitochondrial deficiency in several neurodegenerative diseases [106]. The mechanisms linking mitochondrial deficiency neurodegeneration are not yet clear. In the present study, we studied the neuronal morphology of mitochondrial deficient nematodes. We identified a signaling pathway that connects mitochondrial impairment with altered neuronal architecture. Specifically, we showed that *C. elegans* mutant strains lacking the mitochondrial Complex I display increased dendritic arborizations of their mechanosensory neurons in a non-cell-type specific manner. Given that the increased dendritic branching is not abolished by treatment with antioxidants, we ruled out that increased oxidative stress participates in this process. The observed branching potentiation is being regulated by a signaling pathway formed by AMP-activated protein kinase and PI3 kinase. Finally, our findings demonstrate that the increased neuronal branching of OXPHOS impaired animals is uncoupled from accelerated ageing.

In our study we demonstrated that the potentiation of branching in OXPHOS impairment conditions is mediated by the AMPK/PI3K axis. This is in agreement with previous findings showing that these two proteins can regulate neuronal branching in other systems. For example, overexpression of the serine threonine kinase LKB1 controls axon specification and branching through the activation of the AMPK-like kinase NUAK1 and the consequent immobilization of mitochondria at the nascent presynaptic site [28]. Although the role of AMPK activation in neuronal polarization, axogenesis and axon growth has been a topic of debate, overall the general notion is that AMPK activation levels affect neuronal polarization [107, 108]. Furthermore, AICAR-mediated AMPK activation prevents PI3K localization and Akt activity at the neurite tips during development. This results into suppression of axonal growth and neuronal polarization [103]. Although we also showed the involvement of PI3K, AMPK overactivation due to AICAR treatment in our setting led to excessive branching rather than reduced polarization. The difference between our and the aforementioned findings could derive from differences in the two studied models (*C. elegans* mechanosensory neurons versus hippocampal neurons) as well as the focus of the cellular compartment (dendrites versus axons).

AMPK has a great variety of downstream targets [109]. One that is of high interest is the peroxisome proliferator-activated receptor γ co-activator 1α (PGC-1α) which is a master regulator of mitochondrial biogenesis [110-112]. Multiple lines of evidence suggest that AMPK activates this factor thereby increasing mitochondrial biogenesis [113-115]. Although the *C. elegans* genome lacks the orthologs of PGC-1α proteins [116], according to the above

evidence, one of our speculations is that activation of AMPK (in our setting either via AICAR treatment or mitochondrial deficiency) could activate the protein(s) that have a PGC-1α-like function in *C. elegans* [117]. This could be one of the reasons underlying the excessive neuronal branching since PGC-1α is also involved in the formation and maintenance of neuronal dendritic spines in mammalian neurons [118]. The hypothesis of the involvement of an AMPK-activated protein stimulating mitochondrial biogenesis would fit for a second reason: increased mitochondrial numbers could contribute to the increase of immobilized mitochondria that are capable of inducing branching formation as discussed above [28].

Overall, AMPK serves as an energy sensor and low energy levels can activate it leading to increased glucose transport, fatty acid oxidation and mitochondrial biogenesis [119]. As shown in our study, AMPK is activated as a response to mitochondrial deficiency. Since mitochondrial deficiency is increasingly linked to neurodegenerative diseases [120, 121], the consequential activation of AMPK is considered important as a therapeutic target. Indeed, AMPK can be pharmacologically modulated [122] and its involvement in neurodegeneration has been extensively studied [123]. For example, several studies have shown that by treating mouse models of Alzheimer's disease with AMPK activators can upregulate the expression of autophagy-related proteins and improve their memory (reviewed in [124]). Our findings prove the connection of mitochondrial deficiency with AMPK activation, highlight the role of AMPK in neuronal architecture –which is affected during neurodegeneration [12, 13]- and show how mitochondrial deficiency, which can occur in neurodegenerative diseases, triggers a metabolic pathway that alters the shape of neurons.

Formation of additional dendritic branches under energy deprivation circumstances caused by mitochondrial impairment is rather counterintuitive. Perhaps changes in the mitochondrial network due to the respiratory deficiency might affect dendritic branching. Alternatively, growth of additional dendritic branches could be the result of compensation due to reduced functionality of the neuron. This could be attributed to the reduced activity of channels on the surface of the neuron which can enhance branching of the neuron.

Regarding the first interpretation about changes in mitochondrial network, it has been shown that Complex IV deficiency can lead to mitochondrial hyperfusion [125]. Such an event can deprive the cells of small motile mitochondria, which in the case of the highly polarized neuronal cells are of high importance. Indeed, increased mitochondrial fusion affects the formation of neurites and spines as demonstrated in mammalian neurons [24]. Similarly, in our setting, increased mitochondrial fusion of Complex I mutants can be a contributing factor

to the increased (in the case of PVD neurons) or ectopic (in the case of PLM neurons) branching. In addition, mitochondrial motility can affect neuronal morphology. According to observations from cortical neurons both *in vivo* and *in vitro*, immobile mitochondria can stimulate branching whereas mobile mitochondria lack this capacity [28]. Indeed, the presence of mitochondria in presumptive branching points facilitates the energy required for protein synthesis and calcium buffering, which contributes to actin-dependent branching initiation [126]. In our experimental setup, comparison of mitochondrial dynamics, trafficking and size in the neurons of wild type and OXPHOS impairment mutants could give more information on the validity of this hypothesis.

Our alternative hypothesis on the increased branching as a process to compensate reduced functionality is interesting, yet difficult to confirm. It has been demonstrated that reduced voltage activated channel activity in sensory neurons can potentiate excessive branching in certain neurons of *C. elegans* [127, 128]. This is explained by the reduced sensitivity of the neuron which is incapable of recognizing its final target and therefore receiving the signals that inhibit its growth. The voltage activated channels require Ca^{2+} buffering [129] to which mitochondria significantly contribute. On the basis of evidence indicating that under conditions of mitochondrial deficiency, mitochondria have altered Ca^{2+} buffering capacity [130], the function of voltage gated channels could be compromised thus resulting in lack of sensitivity of the neuron and consequent excessive or ectopic branching. Addressing this question in our setup can be quite challenging. A potential approach would be the generation of a transgenic *C. elegans* strain overexpressing a channelrhodopsin and a genetically encoded Ca^{2+} reporter in the PVD neurons. Light stimulation of the channelrhodopsin-expressing PVD neuron would cause a Ca^{2+} transient in the neuron which can be measured by a genetically encoded Ca^{2+} reporter [131, 132]. Assuming that the enhanced neuronal branching in OXPHOS mutants is a compensatory mechanism one would expect to see comparable neuronal activities between wild type and OXPHOS impairment mutants. Nevertheless, this would indicate that the excessive branching is a compensatory mechanism and would not prove it since perhaps the neuronal functionality of OXPHOS mutants is not affected. One way to overcome this obstacle would be to compare neuronal activities between *aak-2* and *gas-1; aak-2* mutants. *aak-2* mutants have neurons structurally comparable to wild type animals and additionally the *gas-1; aak-2* double mutants, although they are OXPHOS mutants do not display extra dendritic arborizations. If the excessive branching is indeed compensating for functionality loss, *gas-1; aak-2* double mutants should display reduced

activity compared to *aak-2* single mutants since the *aak-2* mutation in the *gas-1* genetic background inhibits the formation of excessive neuronal outgrowths.

Apart from the two main speculation lines discussed above, several other scenarios are possible. For instance, the observed branching potentiation due to OXPHOS impairment could be the result of the combination of various factors. Perhaps the expression of molecules regulating dendritic branching is affected. In addition, our data do not clarify if the observed effect is cell- or non cell-autonomous. Therefore, a deeper analysis of the contribution of branching regulators in the observed phenotype could partly elucidate the relation between metabolic changes and cell shaping molecules. To that end, determining if the altered neuronal architecture of OXPHOS mutants is a cell or non-cell autonomous phenomenon could indicate whether the cell shaping molecules participating in the remodeling act in an intra- or extracellular manner.

Finally, our data demonstrate that the increased neuronal branching due to mitochondrial deficiency is not related to ageing. Other studies have also shown that ageing affects neuronal branching in *C. elegans* and this alteration is characterized by the presence of extra neuronal processes on touch receptor neurons [62, 63]. Tank *et al.* observed accelerated neurite branching in short-lived mitochondrial deficiency mutant animals and they attributed that to the accelerated ageing. In addition, they showed that long-lived mitochondrial mutants exhibit delayed onset of extra neuronal projections. Nevertheless, we showed that young adult animals with similar mitochondrial deficiencies have extra neuronal processes and this occurs regardless of their lifespan duration. The contradiction between the two studies could be due to the fact that Toth *et al.* do not provide measurements of young adult animals that carry mitochondrial deficiencies, but only measurements from day 10 adult animals. Examining neuronal morphology of animals this stage could lead to a misinterpretation of the presence of ectopic neuronal projections as an effect of accelerated ageing and not of mitochondrial deficiency.

The remarkable age-related phenotype of the PVD neuron is quite intriguing. Ageing is associated with cognitive function decline in humans, and this can be partly explained by alterations in neuronal morphology of the ageing brain. Although the concept of extra neuronal processes forming due to ageing seems counterintuitive, it has been reported that in some brain areas of humans the dendritic extent of neurons can be greater in aged individuals compared to younger ones [133, 134]. Since the *C. elegans* nervous system demonstrates

similar changes, it could be used as a model to reveal the mechanisms underlying age-related alterations of neuronal architecture.

In summary, with this work we developed and described a new animal model for the analysis of dendritic branching under conditions of OXPHOS impairment. We revealed a novel signaling pathway that regulates neuronal branching under mitochondrial deficiency conditions, although more work is required to uncover the rest of the players participating in this signaling cascade. A closer look at mitochondrial dynamics, trafficking, and the role of neuronal branching regulators could potentially yield conclusions relevant for the elucidation of mechanisms underlying neurodegenerative diseases.

6. List of abbreviations

ADP: Adenosine diphosphate

AICAR: 5-Aminoimidazole-4-carboxamide ribonucleotide

AMP: Adenosine monophosphate

AMPK: AMP-activated protein kinase

APL-1: Amyloid precursor-like

APP: Amyloid precursor protein

APS: ammonium persulfate

ATP: Adenosine triphosphate

Aβ: Amyloid beta

BSA: Bovine serum albumin

C. elegans: *Caenorhabditis elegans*

CPEB1: Cytoplasmic Polyadenylation Element Binding Protein 1

DNA: Deoxyribonucleic acid

dNTPs: Deoxynucleotides triphosphates

ECL: Enhanced chemiluminescence

E. Coli: *Escherichia coli*

et al.: And others ("et alii")

GFP: Green fluorescent protein

HTT: huntingtin

LacZ: β-galactosidase of the lactose operon

LB: Lysogeny broth

LKB1: Liver kinase 1

mL: milli liter

mm: milli meter

mRNA: messenger RNA (Ribonucleic acid)

mV: mili volt

NGM: nematode growth medium

nm: nano meter

OXPHOS: Oxidative phosphorylation

PAGE: Polyacrylamide gel electrophoresis

PCR: Polymerase chain reaction

PGC-1α: Peroxisome Proliferator-activated receptor γ co-activator 1α

PI3K: Phosphatidylinositol-4,5-biphosphate 3-kinase

RIPA: Radio-immunoprecipitation assay

RNAi: RNA interference

rpm: rounds per minute

SDS: sodium dodecyl sulfate

Taq: *Thermus aquaticus*

TBE: Tris/Borate/EDTA

TBS: Tris-buffered saline

TEMED: Tetramethylethylenediamine

U: Unit

ZEN: Zeiss efficient navigation

µL: micro liter

µM: micro molar

% (v/v): volume/volume percentage

% (w/v): weight/volume percentage

7. References

1. Andres-Barquin, P.J., *Ramon y Cajal: a century after the publication of his masterpiece.* Endeavour, 2001. **25**(1): p. 13-7.
2. Yoshimura, T., N. Arimura, and K. Kaibuchi, *Molecular mechanisms of axon specification and neuronal disorders.* Ann N Y Acad Sci, 2006. **1086**: p. 116-25.
3. Lalli, G., *Regulation of neuronal polarity.* Exp Cell Res, 2014.
4. Lewis, T.L., Jr., J. Courchet, and F. Polleux, *Cell biology in neuroscience: Cellular and molecular mechanisms underlying axon formation, growth, and branching.* J Cell Biol, 2013. **202**(6): p. 837-48.
5. Tau, G.Z. and B.S. Peterson, *Normal development of brain circuits.* Neuropsychopharmacology, 2010. **35**(1): p. 147-68.
6. McKhann, G.M., *Changing concepts of Alzheimer disease.* JAMA, 2011. **305**(23): p. 2458-9.
7. Turner, R.S., et al., *Amyloids beta40 and beta42 are generated intracellularly in cultured human neurons and their secretion increases with maturation.* J Biol Chem, 1996. **271**(15): p. 8966-70.
8. Mandelkow, E.M. and E. Mandelkow, *Tau in Alzheimer's disease.* Trends Cell Biol, 1998. **8**(11): p. 425-7.
9. Brown, R.G. and C.D. Marsden, *Cognitive function in Parkinson's disease: from description to theory.* Trends Neurosci, 1990. **13**(1): p. 21-9.
10. Forno, L.S., *Neuropathology of Parkinson's disease.* J Neuropathol Exp Neurol, 1996. **55**(3): p. 259-72.
11. Thomas, B. and M.F. Beal, *Parkinson's disease.* Hum Mol Genet, 2007. **16 Spec No. 2**: p. R183-94.
12. Arendt, T., et al., *Dendritic reorganisation in the basal forebrain under degenerative conditions and its defects in Alzheimer's disease. II. Ageing, Korsakoff's disease, Parkinson's disease, and Alzheimer's disease.* J Comp Neurol, 1995. **351**(2): p. 189-222.
13. Krstic, D. and I. Knuesel, *Deciphering the mechanism underlying late-onset Alzheimer disease.* Nat Rev Neurol, 2013. **9**(1): p. 25-34.
14. Rikani, A.A., et al., *The mechanism of degeneration of striatal neuronal subtypes in Huntington disease.* Ann Neurosci, 2014. **21**(3): p. 112-114.
15. Roze, E., et al., *Huntington's disease.* Adv Exp Med Biol, 2010. **685**: p. 45-63.
16. Graveland, G.A., R.S. Williams, and M. DiFiglia, *Evidence for degenerative and regenerative changes in neostriatal spiny neurons in Huntington's disease.* Science, 1985. **227**(4688): p. 770-3.
17. Ferrante, R.J., N.W. Kowall, and E.P. Richardson, Jr., *Proliferative and degenerative changes in striatal spiny neurons in Huntington's disease: a combined study using the section-Golgi method and calbindin D28k immunocytochemistry.* J Neurosci, 1991. **11**(12): p. 3877-87.
18. Mayeux, R., *Epidemiology of neurodegeneration.* Annu Rev Neurosci, 2003. **26**: p. 81-104.
19. Beal, M.F., *Mitochondrial dysfunction in neurodegenerative diseases.* Biochim Biophys Acta, 1998. **1366**(1-2): p. 211-23.
20. Mitchell, P., *Chemiosmotic coupling in oxidative and photosynthetic phosphorylation. 1966.* Biochim Biophys Acta, 2011. **1807**(12): p. 1507-38.
21. Oruganty-Das, A., et al., *Translational control of mitochondrial energy production mediates neuron morphogenesis.* Cell Metab, 2012. **16**(6): p. 789-800.

22. Lackner, L.L., *Shaping the dynamic mitochondrial network.* BMC Biol, 2014. **12**: p. 35.
23. Scott, S.V., et al., *Staying in aerobic shape: how the structural integrity of mitochondria and mitochondrial DNA is maintained.* Curr Opin Cell Biol, 2003. **15**(4): p. 482-8.
24. Li, Z., et al., *The importance of dendritic mitochondria in the morphogenesis and plasticity of spines and synapses.* Cell, 2004. **119**(6): p. 873-87.
25. Ishihara, N., et al., *Mitochondrial fission factor Drp1 is essential for embryonic development and synapse formation in mice.* Nat Cell Biol, 2009. **11**(8): p. 958-66.
26. Chen, H., J.M. McCaffery, and D.C. Chan, *Mitochondrial fusion protects against neurodegeneration in the cerebellum.* Cell, 2007. **130**(3): p. 548-62.
27. Glater, E.E., et al., *Axonal transport of mitochondria requires milton to recruit kinesin heavy chain and is light chain independent.* J Cell Biol, 2006. **173**(4): p. 545-57.
28. Courchet, J., et al., *Terminal axon branching is regulated by the LKB1-NUAK1 kinase pathway via presynaptic mitochondrial capture.* Cell, 2013. **153**(7): p. 1510-25.
29. Lin, M.T. and M.F. Beal, *Mitochondrial dysfunction and oxidative stress in neurodegenerative diseases.* Nature, 2006. **443**(7113): p. 787-95.
30. DiMauro, S. and E.A. Schon, *Mitochondrial respiratory-chain diseases.* N Engl J Med, 2003. **348**(26): p. 2656-68.
31. Nunomura, A., et al., *Oxidative damage is the earliest event in Alzheimer disease.* J Neuropathol Exp Neurol, 2001. **60**(8): p. 759-67.
32. Pratico, D., et al., *Increased lipid peroxidation precedes amyloid plaque formation in an animal model of Alzheimer amyloidosis.* J Neurosci, 2001. **21**(12): p. 4183-7.
33. Stokin, G.B., et al., *Axonopathy and transport deficits early in the pathogenesis of Alzheimer's disease.* Science, 2005. **307**(5713): p. 1282-8.
34. Wang, X., et al., *The role of abnormal mitochondrial dynamics in the pathogenesis of Alzheimer's disease.* J Neurochem, 2009. **109 Suppl 1**: p. 153-9.
35. Calkins, M.J., et al., *Impaired mitochondrial biogenesis, defective axonal transport of mitochondria, abnormal mitochondrial dynamics and synaptic degeneration in a mouse model of Alzheimer's disease.* Hum Mol Genet, 2011. **20**(23): p. 4515-29.
36. Schapira, A.H., et al., *Mitochondrial complex I deficiency in Parkinson's disease.* Lancet, 1989. **1**(8649): p. 1269.
37. Chen, H. and D.C. Chan, *Mitochondrial dynamics--fusion, fission, movement, and mitophagy--in neurodegenerative diseases.* Hum Mol Genet, 2009. **18**(R2): p. R169-76.
38. Kim, J., et al., *Mitochondrial loss, dysfunction and altered dynamics in Huntington's disease.* Hum Mol Genet, 2010. **19**(20): p. 3919-35.
39. Pandey, M., K.P. Mohanakumar, and R. Usha, *Mitochondrial functional alterations in relation to pathophysiology of Huntington's disease.* J Bioenerg Biomembr, 2010. **42**(3): p. 217-26.
40. Choo, Y.S., et al., *Mutant huntingtin directly increases susceptibility of mitochondria to the calcium-induced permeability transition and cytochrome c release.* Hum Mol Genet, 2004. **13**(14): p. 1407-20.
41. Yano, H., et al., *Inhibition of mitochondrial protein import by mutant huntingtin.* Nat Neurosci, 2014. **17**(6): p. 822-31.
42. Gu, M., et al., *Mitochondrial defect in Huntington's disease caudate nucleus.* Ann Neurol, 1996. **39**(3): p. 385-9.
43. Shirendeb, U.P., et al., *Mutant huntingtin's interaction with mitochondrial protein Drp1 impairs mitochondrial biogenesis and causes defective axonal transport and synaptic degeneration in Huntington's disease.* Hum Mol Genet, 2012. **21**(2): p. 406-20.

44. Brenner, S., *The genetics of Caenorhabditis elegans.* Genetics, 1974. **77**(1): p. 71-94.
45. Hekimi, S., et al., *Molecular genetics of life span in C. elegans: how much does it teach us?* Trends Genet, 1998. **14**(1): p. 14-20.
46. Lapierre, L.R. and M. Hansen, *Lessons from C. elegans: signaling pathways for longevity.* Trends Endocrinol Metab, 2012. **23**(12): p. 637-44.
47. Hobert, O., *Specification of the nervous system.* WormBook, 2005: p. 1-19.
48. Hobert, O., *Neurogenesis in the nematode Caenorhabditis elegans.* WormBook, 2010: p. 1-24.
49. Fay, D.S., *The cell cycle and development: lessons from C. elegans.* Semin Cell Dev Biol, 2005. **16**(3): p. 397-406.
50. Mallo, G.V., et al., *Inducible antibacterial defense system in C. elegans.* Curr Biol, 2002. **12**(14): p. 1209-14.
51. Kurz, C.L. and J.J. Ewbank, *Caenorhabditis elegans: an emerging genetic model for the study of innate immunity.* Nat Rev Genet, 2003. **4**(5): p. 380-90.
52. Kaletta, T. and M.O. Hengartner, *Finding function in novel targets: C. elegans as a model organism.* Nat Rev Drug Discov, 2006. **5**(5): p. 387-98.
53. Giacomotto, J. and L. Segalat, *High-throughput screening and small animal models, where are we?* Br J Pharmacol, 2010. **160**(2): p. 204-16.
54. Lai, C.H., et al., *Identification of novel human genes evolutionarily conserved in Caenorhabditis elegans by comparative proteomics.* Genome Res, 2000. **10**(5): p. 703-13.
55. Markaki, M. and N. Tavernarakis, *Modeling human diseases in Caenorhabditis elegans.* Biotechnol J, 2010. **5**(12): p. 1261-76.
56. Rieckher, M., et al., *Transgenesis in Caenorhabditis elegans.* Methods Mol Biol, 2009. **561**: p. 21-39.
57. White, J.G., et al., *The structure of the nervous system of the nematode Caenorhabditis elegans.* Philos Trans R Soc Lond B Biol Sci, 1986. **314**(1165): p. 1-340.
58. Ward, S., et al., *Electron microscopical reconstruction of the anterior sensory anatomy of the nematode Caenorhabditis elegans.?2UU.* J Comp Neurol, 1975. **160**(3): p. 313-37.
59. Way, J.C. and M. Chalfie, *The mec-3 gene of Caenorhabditis elegans requires its own product for maintained expression and is expressed in three neuronal cell types.* Genes Dev, 1989. **3**(12A): p. 1823-33.
60. Chalfie, M., et al., *Green fluorescent protein as a marker for gene expression.* Science, 1994. **263**(5148): p. 802-5.
61. Peng, C.Y., et al., *C. elegans model of neuronal aging.* Commun Integr Biol, 2011. **4**(6): p. 696-8.
62. Tank, E.M., K.E. Rodgers, and C. Kenyon, *Spontaneous age-related neurite branching in Caenorhabditis elegans.* J Neurosci, 2011. **31**(25): p. 9279-88.
63. Toth, M.L., et al., *Neurite sprouting and synapse deterioration in the aging Caenorhabditis elegans nervous system.* J Neurosci, 2012. **32**(26): p. 8778-90.
64. Yanik, M.F., et al., *Neurosurgery: functional regeneration after laser axotomy.* Nature, 2004. **432**(7019): p. 822.
65. Kage, E., et al., *MBR-1, a novel helix-turn-helix transcription factor, is required for pruning excessive neurites in Caenorhabditis elegans.* Curr Biol, 2005. **15**(17): p. 1554-9.
66. Bargmann, C.I., *Neurobiology of the Caenorhabditis elegans genome.* Science, 1998. **282**(5396): p. 2028-33.

67. Sawin, E.R., R. Ranganathan, and H.R. Horvitz, *C. elegans locomotory rate is modulated by the environment through a dopaminergic pathway and by experience through a serotonergic pathway.* Neuron, 2000. **26**(3): p. 619-31.
68. Hobert, O., *Behavioral plasticity in C. elegans: paradigms, circuits, genes.* J Neurobiol, 2003. **54**(1): p. 203-23.
69. Smith, C.J., et al., *Time-lapse imaging and cell-specific expression profiling reveal dynamic branching and molecular determinants of a multi-dendritic nociceptor in C. elegans.* Dev Biol, 2010. **345**(1): p. 18-33.
70. Albeg, A., et al., *C. elegans multi-dendritic sensory neurons: morphology and function.* Mol Cell Neurosci, 2011. **46**(1): p. 308-17.
71. Smith, C.J., et al., *Netrin (UNC-6) mediates dendritic self-avoidance.* Nat Neurosci, 2012. **15**(5): p. 731-7.
72. Liu, O.W. and K. Shen, *The transmembrane LRR protein DMA-1 promotes dendrite branching and growth in C. elegans.* Nat Neurosci, 2012. **15**(1): p. 57-63.
73. Dong, X., et al., *An extracellular adhesion molecule complex patterns dendritic branching and morphogenesis.* Cell, 2013. **155**(2): p. 296-307.
74. Wolozin, B., et al., *Watching worms whither: modeling neurodegeneration in C. elegans.* Prog Mol Biol Transl Sci, 2011. **100**: p. 499-514.
75. Li, J. and W. Le, *Modeling neurodegenerative diseases in Caenorhabditis elegans.* Exp Neurol, 2013. **250**: p. 94-103.
76. Johnson, J.R., et al., *Caenorhabditis elegans: a useful tool to decipher neurodegenerative pathways.* Biochem Soc Trans, 2010. **38**(2): p. 559-63.
77. Dosanjh, L.E., et al., *Behavioral phenotyping of a transgenic Caenorhabditis elegans expressing neuronal amyloid-beta.* J Alzheimers Dis, 2010. **19**(2): p. 681-90.
78. Wentzell, J. and D. Kretzschmar, *Alzheimer's disease and tauopathy studies in flies and worms.* Neurobiol Dis, 2010. **40**(1): p. 21-8.
79. Wiese, M., A. Antebi, and H. Zheng, *Intracellular trafficking and synaptic function of APL-1 in Caenorhabditis elegans.* PLoS One, 2010. **5**(9).
80. Lakso, M., et al., *Dopaminergic neuronal loss and motor deficits in Caenorhabditis elegans overexpressing human alpha-synuclein.* J Neurochem, 2003. **86**(1): p. 165-72.
81. Dauer, W. and C.C. Ho, *The biology and pathology of the familial Parkinson's disease protein LRRK2.* Mov Disord, 2010. **25 Suppl 1**: p. S40-3.
82. Saha, S., et al., *LRRK2 modulates vulnerability to mitochondrial dysfunction in Caenorhabditis elegans.* J Neurosci, 2009. **29**(29): p. 9210-8.
83. Faber, P.W., et al., *Polyglutamine-mediated dysfunction and apoptotic death of a Caenorhabditis elegans sensory neuron.* Proc Natl Acad Sci U S A, 1999. **96**(1): p. 179-84.
84. Parker, J.A., et al., *Expanded polyglutamines in Caenorhabditis elegans cause axonal abnormalities and severe dysfunction of PLM mechanosensory neurons without cell death.* Proc Natl Acad Sci U S A, 2001. **98**(23): p. 13318-23.
85. Sin, O., H. Michels, and E.A. Nollen, *Genetic screens in Caenorhabditis elegans models for neurodegenerative diseases.* Biochim Biophys Acta, 2014. **1842**(10): p. 1951-1959.
86. Ventura, N. and S.L. Rea, *Caenorhabditis elegans mitochondrial mutants as an investigative tool to study human neurodegenerative diseases associated with mitochondrial dysfunction.* Biotechnol J, 2007. **2**(5): p. 584-95.
87. Tsalik, E.L., et al., *LIM homeobox gene-dependent expression of biogenic amine receptors in restricted regions of the C. elegans nervous system.* Dev Biol, 2003. **263**(1): p. 81-102.

88. Kayser, E.B., P.G. Morgan, and M.M. Sedensky, *GAS-1: a mitochondrial protein controls sensitivity to volatile anesthetics in the nematode Caenorhabditis elegans.* Anesthesiology, 1999. **90**(2): p. 545-54.
89. Kayser, E.B., et al., *Mitochondrial expression and function of GAS-1 in Caenorhabditis elegans.* J Biol Chem, 2001. **276**(23): p. 20551-8.
90. Yang, W. and S. Hekimi, *Two modes of mitochondrial dysfunction lead independently to lifespan extension in Caenorhabditis elegans.* Aging Cell, 2010. **9**(3): p. 433-47.
91. Yang, W. and S. Hekimi, *A mitochondrial superoxide signal triggers increased longevity in Caenorhabditis elegans.* PLoS Biol, 2010. **8**(12): p. e1000556.
92. Hekimi, S., J. Lapointe, and Y. Wen, *Taking a "good" look at free radicals in the aging process.* Trends Cell Biol, 2011. **21**(10): p. 569-76.
93. Padayatty, S.J., et al., *Vitamin C as an antioxidant: evaluation of its role in disease prevention.* J Am Coll Nutr, 2003. **22**(1): p. 18-35.
94. Clark, S.G. and C. Chiu, *C. elegans ZAG-1, a Zn-finger-homeodomain protein, regulates axonal development and neuronal differentiation.* Development, 2003. **130**(16): p. 3781-94.
95. Viscomi, C., et al., *In vivo correction of COX deficiency by activation of the AMPK/PGC-1alpha axis.* Cell Metab, 2011. **14**(1): p. 80-90.
96. Li, L., Y. Chen, and S.B. Gibson, *Starvation-induced autophagy is regulated by mitochondrial reactive oxygen species leading to AMPK activation.* Cell Signal, 2013. **25**(1): p. 50-65.
97. Hardie, D.G., *AMP-activated protein kinase: an energy sensor that regulates all aspects of cell function.* Genes Dev, 2011. **25**(18): p. 1895-908.
98. Apfeld, J., et al., *The AMP-activated protein kinase AAK-2 links energy levels and insulin-like signals to lifespan in C. elegans.* Genes Dev, 2004. **18**(24): p. 3004-9.
99. Curtis, R., G. O'Connor, and P.S. DiStefano, *Aging networks in Caenorhabditis elegans: AMP-activated protein kinase (aak-2) links multiple aging and metabolism pathways.* Aging Cell, 2006. **5**(2): p. 119-26.
100. Golubitzky, A., et al., *Screening for active small molecules in mitochondrial complex I deficient patient's fibroblasts, reveals AICAR as the most beneficial compound.* PLoS One, 2011. **6**(10): p. e26883.
101. Shi, S.H., L.Y. Jan, and Y.N. Jan, *Hippocampal neuronal polarity specified by spatially localized mPar3/mPar6 and PI 3-kinase activity.* Cell, 2003. **112**(1): p. 63-75.
102. Menager, C., et al., *PIP3 is involved in neuronal polarization and axon formation.* J Neurochem, 2004. **89**(1): p. 109-18.
103. Amato, S., et al., *AMP-activated protein kinase regulates neuronal polarization by interfering with PI 3-kinase localization.* Science, 2011. **332**(6026): p. 247-51.
104. Morris, J.Z., H.A. Tissenbaum, and G. Ruvkun, *A phosphatidylinositol-3-OH kinase family member regulating longevity and diapause in Caenorhabditis elegans.* Nature, 1996. **382**(6591): p. 536-9.
105. Kenyon, C., et al., *A C. elegans mutant that lives twice as long as wild type.* Nature, 1993. **366**(6454): p. 461-4.
106. Chaturvedi, R.K. and M. Flint Beal, *Mitochondrial diseases of the brain.* Free Radic Biol Med, 2013. **63**: p. 1-29.
107. Dasgupta, B. and J. Milbrandt, *AMP-activated protein kinase phosphorylates retinoblastoma protein to control mammalian brain development.* Dev Cell, 2009. **16**(2): p. 256-70.
108. Williams, T., et al., *AMP-activated protein kinase (AMPK) activity is not required for neuronal development but regulates axogenesis during metabolic stress.* Proc Natl Acad Sci U S A, 2011. **108**(14): p. 5849-54.

109. Hardie, D.G., et al., *Management of cellular energy by the AMP-activated protein kinase system.* FEBS Lett, 2003. **546**(1): p. 113-20.
110. Wu, Z., et al., *Mechanisms controlling mitochondrial biogenesis and respiration through the thermogenic coactivator PGC-1.* Cell, 1999. **98**(1): p. 115-24.
111. Lehman, J.J., et al., *Peroxisome proliferator-activated receptor gamma coactivator-1 promotes cardiac mitochondrial biogenesis.* J Clin Invest, 2000. **106**(7): p. 847-56.
112. Puigserver, P. and B.M. Spiegelman, *Peroxisome proliferator-activated receptor-gamma coactivator 1 alpha (PGC-1 alpha): transcriptional coactivator and metabolic regulator.* Endocr Rev, 2003. **24**(1): p. 78-90.
113. Lee, W.J., et al., *AMPK activation increases fatty acid oxidation in skeletal muscle by activating PPARalpha and PGC-1.* Biochem Biophys Res Commun, 2006. **340**(1): p. 291-5.
114. Yu, L. and S.J. Yang, *AMP-activated protein kinase mediates activity-dependent regulation of peroxisome proliferator-activated receptor gamma coactivator-1alpha and nuclear respiratory factor 1 expression in rat visual cortical neurons.* Neuroscience, 2010. **169**(1): p. 23-38.
115. Ashabi, G., et al., *Activation of AMP-activated protein kinase by metformin protects against global cerebral ischemia in male rats: interference of AMPK/PGC-1alpha pathway.* Metab Brain Dis, 2014. **29**(1): p. 47-58.
116. Knutti, D., A. Kaul, and A. Kralli, *A tissue-specific coactivator of steroid receptors, identified in a functional genetic screen.* Mol Cell Biol, 2000. **20**(7): p. 2411-22.
117. Taubert, S., et al., *A Mediator subunit, MDT-15, integrates regulation of fatty acid metabolism by NHR-49-dependent and -independent pathways in C. elegans.* Genes Dev, 2006. **20**(9): p. 1137-49.
118. Cheng, A., et al., *Involvement of PGC-1alpha in the formation and maintenance of neuronal dendritic spines.* Nat Commun, 2012. **3**: p. 1250.
119. Shirwany, N.A. and M.H. Zou, *AMPK: a cellular metabolic and redox sensor. A minireview.* Front Biosci (Landmark Ed), 2014. **19**: p. 447-74.
120. Zsurka, G. and W.S. Kunz, *Mitochondrial involvement in neurodegenerative diseases.* IUBMB Life, 2013. **65**(3): p. 263-72.
121. Cavallucci, V., A. Nobili, and M. D'Amelio, *Emerging role of mitochondria dysfunction in the onset of neurodegenerative diseases.* J Biol Regul Homeost Agents, 2013. **27**(2 Suppl): p. 1-9.
122. Yun, H. and J. Ha, *AMP-activated protein kinase modulators: a patent review (2006 - 2010).* Expert Opin Ther Pat, 2011. **21**(7): p. 983-1005.
123. Spasic, M.R., P. Callaerts, and K.K. Norga, *AMP-activated protein kinase (AMPK) molecular crossroad for metabolic control and survival of neurons.* Neuroscientist, 2009. **15**(4): p. 309-16.
124. Godoy, J.A., et al., *Signaling pathway cross talk in Alzheimer's disease.* Cell Commun Signal, 2014. **12**: p. 23.
125. Rolland, S.G., et al., *Impaired complex IV activity in response to loss of LRPPRC function can be compensated by mitochondrial hyperfusion.* Proc Natl Acad Sci U S A, 2013. **110**(32): p. E2967-76.
126. Spillane, M., et al., *Mitochondria coordinate sites of axon branching through localized intra-axonal protein synthesis.* Cell Rep, 2013. **5**(6): p. 1564-75.
127. Coburn, C.M. and C.I. Bargmann, *A putative cyclic nucleotide-gated channel is required for sensory development and function in C. elegans.* Neuron, 1996. **17**(4): p. 695-706.
128. Coburn, C.M., et al., *A cyclic nucleotide-gated channel inhibits sensory axon outgrowth in larval and adult Caenorhabditis elegans: a distinct pathway for maintenance of sensory axon structure.* Development, 1998. **125**(2): p. 249-58.

129. Kaupp, U.B. and R. Seifert, *Cyclic nucleotide-gated ion channels.* Physiol Rev, 2002. **82**(3): p. 769-824.
130. Dell'agnello, C., et al., *Increased longevity and refractoriness to Ca(2+)-dependent neurodegeneration in Surf1 knockout mice.* Hum Mol Genet, 2007. **16**(4): p. 431-44.
131. Husson, S.J., et al., *Optogenetic analysis of a nociceptor neuron and network reveals ion channels acting downstream of primary sensors.* Curr Biol, 2012. **22**(9): p. 743-52.
132. Schmitt, C., et al., *Specific expression of channelrhodopsin-2 in single neurons of Caenorhabditis elegans.* PLoS One, 2012. **7**(8): p. e43164.
133. Flood, D.G., et al., *Age-related dendritic growth in dentate gyrus of human brain is followed by regression in the 'oldest old'.* Brain Res, 1985. **345**(2): p. 366-8.
134. Flood, D.G., et al., *Dendritic extent in human dentate gyrus granule cells in normal aging and senile dementia.* Brain Res, 1987. **402**(2): p. 205-16.

8. Acknowledgement

Part of this work was funded by the CoEN initiative. I would like to thank my supervisor Dr. Daniele Bano for the encouragement to push me through this process successfully and the trust he showed in my work. Additionally I would like to thank, Professors Nicotera and, Hoch for agreeing to supervise me, and Professors Pankratz and Stoecker for agreeing to participate in my PhD examination.

I am grateful to all the former and current members of the Bano and Nicotera groups which have been great supporters and collaborators and gave me precious scientific and personal feedback in several occasions. Without them creating a relaxing atmosphere in the laboratory, my work would have been much different.

In addition, I would like to thank Mrs. Steffi Nicolaus from the media kitchen of DZNE for the incredible competence she shows daily in supporting us with her technical assistance. Furthermore, Dr. Ireen Koenig of the DZNE Light Microscopy Facility has been a great teacher in the use of confocal microscopy for the needs of this study. Along with these people I would like to thank all the staff of the DZNE Light Microscopy Facility, Technical Infrastructure and the Information Technology for their precious help whenever I needed it. Mrs. Regina Otto and Mrs. Fabienne Fier have also offered their assistance as former and current, respectively, secretaries of our group.

Last but not least, I would like to thank my family and friends who, although several miles away, have been my greatest funs and faithful supporters. I owe them a lot.